Journal of Visualized Experiments

# Fabrication and Characterisation of Photonic Crystal Slow Light Waveguides and Cavities

--Manuscript Draft--

| | |
|---|---|
| **Manuscript Number:** | JoVE50216R1 |
| **Full Title:** | Fabrication and Characterisation of Photonic Crystal Slow Light Waveguides and Cavities |
| **Article Type:** | Methods Article - JoVE Produced Video |
| **Corresponding Author:** | Christopher Paul Reardon, Ph.D.<br>University of St Andrews<br>St Andrews, Fife UNITED KINGDOM |
| **Corresponding Author Secondary Information:** | |
| **Corresponding Author's Institution:** | University of St Andrews |
| **Corresponding Author's Secondary Institution:** | |
| **First Author:** | Christopher Paul Reardon, Ph.D. |
| **First Author Secondary Information:** | |
| **Order of Authors Secondary Information:** | |
| **Abstract:** | Slow light has been one of the hot topics in the photonics community in the past decade, generating great interest both from a fundamental point of view and for its considerable potential for practical applications. Slow light photonic crystal waveguides, in particular, have played a major part and have been successfully employed for delaying optical signals1-4 and the enhancement of both linear5-7 and nonlinear devices.8-11<br><br>Photonic crystal cavities achieve similar effects to that of slow light waveguides, but over a reduced band-width. These cavities offer high Q-factor/volume ratio, for the realisation of optically12 and electrically13 pumped ultra-low threshold lasers and the enhancement of nonlinear effects.14-16 Furthermore, passive filters17 and modulators18-19 have been demonstrated, exhibiting ultra-narrow line-width, high free-spectral range and record values of low energy consumption.<br><br>To attain these exciting results, a robust repeatable fabrication protocol must be developed. In this paper we take an in-depth look at our fabrication protocol which employs electron-beam lithography for the definition of photonic crystal patterns and uses wet and dry etching techniques. Our optimised fabrication recipe results in photonic crystals that do not suffer from vertical asymmetry and exhibit very good edge-wall roughness. We discuss the results of varying the etching parameters and the detrimental effects that they can have on a device, leading to a diagnostic route that can be taken to identify and eliminate similar issues.<br><br>The key to evaluating slow light waveguides is the passive characterisation of transmission and group index spectra. Various methods have been reported, most notably resolving the Fabry-Perot fringes of the transmission spectrum20-21 and interferometric techniques.22-25 Here, we describe a direct, broadband measurement technique combining spectral interferometry with Fourier transform analysis.26 Our method stands out for its simplicity and power, as we can characterise a bare photonic crystal with access waveguides, without need for on-chip interference |
| **Corresponding Author E-Mail:** | cr39@st-andrews.ac.uk |
| **Other Authors:** | Isabella H Rey |
| | Karl Welna |

| | |
|---|---|
| | Liam O'Faolain |
| | Thomas F Krauss |

Dear Editor,

We are pleased to send you a manuscript for publication in the *Journal of Visualised Experiments*, entitled "Fabrication and characterisation of both photonic crystal slow light waveguides and cavities" by Christopher P. Reardon, Isabella H. Rey, Karl Welna, Liam O'Faolain and Thomas F. Krauss.

The importance and impact of the work can be summarised as follows:

a) Description of a fabrication protocol that we have developed and optimised over a number of years of experience, and which results in the realisation of state-of-the art photonic crystal structures.
b) Description of a simple and robust measurement technique for the characterisation of the dispersive properties of slow light waveguides.
c) Description of a non-intrusive characterisation method for the determination of the intrinsic properties of photonic crystal micro-cavities.

We believe that the readership from the applied physics and photonics community will find the paper of great interest, as it provides a detailed insight into techniques that are well established within our group and which, we believe, would greatly benefit from a visual demonstration as offered by the *Journal of Visualised Experiments.*

As potential referees, we can suggest the following high-ranking scientists in the field of photonics:

| **Name** | **Institution** | **Contact** |
|---|---|---|
| Anand Srinivasan | KTH Royal Institute of Technology | anand@kth.se |
| Marc Sorel | University of Glasgow | Marc.Sorel@glasgow.ac.uk |
| Toshihiko Baba | Yokohama National University | baba@ynu.ac.jp |
| Jonathan Finley | Technische Universitat Munchen | finley@wsi.tum.de |
| Susumu Noda | Kyoto University | snoda@kuee.Kyoto-u.ac.jp |

The authors contributions are summarised as follows: C.P.R. wrote the fabrication section with relevant data provided by L.O'F; I.H.R. wrote the slow light characterisation sections and performed the relative experiments; K.W. wrote the cavities characterisation sections and performed the relative experiments. Overall, C.P.R., I.H.R. and K.W. contributed equally to this work. L.O'F. contributed to the development and optimisation of the techniques; T.F.K. is the group leader and provided support and funding.

Best regards,

Christopher Reardon, Isabella Rey, Karl Welna, Liam O'Faolain and Thomas Krauss

# Fabrication and Characterisation of Photonic Crystal Slow Light Waveguides and Cavities

**Authors:**
Christopher P. Reardon[*], Isabella H. Rey[*], Karl Welna[*], Liam O'Faolain and Thomas F. Krauss

[*]C.P.R., I.H.R. and K.W. contributed equally to this work.

**Authors: institution(s)/affiliation(s) for each author:**

Christopher P. Reardon
SUPA School of Physics & Astronomy, University of St Andrews
St Andrews, Scotland, UK
Tel: 01334 467336
Fax: 01334 463104
cr39@st-andrews.ac.uk

Isabella H. Rey
SUPA School of Physics & Astronomy, University of St Andrews
St Andrews, Scotland, UK
ir21@st-andrews.ac.uk

Karl Welna
SUPA School of Physics & Astronomy, University of St Andrews
St Andrews, Scotland, UK
kw322@st-andrews.ac.uk

Liam O'Faolain (also known as William Whelan-Curtin)
SUPA School of Physics & Astronomy, University of St Andrews
St Andrews, Scotland, UK
jww1@st-andrews.ac.uk

Thomas F. Krauss
SUPA School of Physics & Astronomy, University of St Andrews
St Andrews, Scotland, UK
tfk@st-andrews.ac.uk

**Corresponding author:**

Christopher P. Reardon

**Keywords:**

Photonic Crystals, Slow-light, Cavities, Waveguides, Silicon, SOI, Fabrication, Characterisation

**Short Abstract:** (50 words maximum)

Use of photonic crystal slow light waveguides and cavities has been widely adopted by the photonics community in many differing applications. Therefore fabrication and characterisation of these devices are of great interest. This paper outlines our fabrication technique and two optical characterisation methods, namely: interferometric (waveguides) and resonant scattering (cavities).

**Long Abstract:** (150 words minimum, 400 words maximum)

Slow light has been one of the hot topics in the photonics community in the past decade, generating great interest both from a fundamental point of view and for its considerable potential for practical applications. Slow light photonic crystal waveguides, in particular, have played a major part and have been successfully employed for delaying optical signals[1-4] and the enhancement of both linear[5-7] and nonlinear devices.[8-11]

Photonic crystal cavities achieve similar effects to that of slow light waveguides, but over a reduced band-width. These cavities offer high *Q*-factor/volume ratio, for the realisation of optically[12] and electrically[13] pumped ultra-low threshold lasers and the enhancement of nonlinear effects.[14-16] Furthermore, passive filters[17] and modulators[18-19] have been demonstrated, exhibiting ultra-narrow line-width, high free-spectral range and record values of low energy consumption.

To attain these exciting results, a robust repeatable fabrication protocol must be developed. In this paper we take an in-depth look at our fabrication protocol which employs electron-beam lithography for the definition of photonic crystal patterns and uses wet and dry etching techniques. Our optimised fabrication recipe results in photonic crystals that do not suffer from vertical asymmetry and exhibit very good edge-wall roughness. We discuss the results of varying the etching parameters and the detrimental effects that they can have on a device, leading to a diagnostic route that can be taken to identify and eliminate similar issues.

The key to evaluating slow light waveguides is the passive characterisation of transmission and group index spectra. Various methods have been reported, most notably resolving the Fabry-Perot fringes of the transmission spectrum[20-21] and interferometric techniques.[22-25] Here, we describe a direct, broadband measurement technique combining spectral interferometry with Fourier transform analysis.[26] Our method stands out for its simplicity and power, as we can characterise a bare photonic crystal with access waveguides, without need for on-chip interference components, and the setup only consists of a Mach-Zehnder interferometer, with no need for moving parts and delay scans.

When characterising photonic crystal cavities, techniques involving internal sources[21] or external waveguides directly coupled to the cavity[27] impact on the performance of the cavity itself, thereby distorting the measurement. Here, we describe a novel and non-intrusive technique that makes use of a cross-polarised probe beam and is known as *resonant scattering* (RS), where the probe is coupled out-of plane into the cavity through an objective. The technique was first demonstrated by McCutcheon *et al.*[28] and further developed by Galli *et al.*[29]

**Protocol Text:**

**Disclaimer:** The following protocol gives a general process flow covering the fabrication and characterisation techniques for photonic crystal waveguides and cavities. The process flow is optimised for the specific equipment available in our laboratory, and parameters may differ if other reagents or equipment is used.

**1.) Sample Preparation**

1.1) Sample Cleaving – take the silicon-on-insulator (SOI) wafer and use a diamond scribe to scratch a line approximately 1-2mm long from the edge of the silicon surface, ensuring that the scratch extends over the edge of the wafer. Align the scratch to a straight edge (e.g. that of a microscope slide) and apply even positive pressure to both sides of the scratch: the wafer will cleave along the crystal plane at the scratch location. Repeat this procedure to define the entire chip.

1.2) Sample Cleaning –. Place the sample into the CAUTION acetone using tweezers and clean in an ultrasonic bath for 1-2min. Remove the sample from the acetone; rinse any remaining acetone from the sample using CAUTION isopropanol (30s) (both acetone and isopropanol are flammable: use good ventilation and avoid all ignition sources). Dry the sample using a clean dry nitrogen gun.

1.3) Spin resist – place the sample onto the spin-coater. Pipette electron sensitive resist CAUTION ZEP520A (ZEP520A is flammable, harmful by inhalation and contact with skin and eyes should be avoided) onto the sample – use enough resist to completely cover the sample without the resist flowing over the edge. Spin the sample so as to give an approx. 350nm thick film and bake on a hotplate at 180$^{o}$C for 10min. We found this thickness to be the optimal thickness that balances resolution and etch resistance (see later).

**2.) Pattern Definition**

2.1) Design – using appropriate software, simulate the required photonic crystal pattern. A number of useful software packages are available, including but not limited to: MIT Photonic Bands (MPB), FullWAVE™ (RSoft), MIT Electromagnetic Equation Propagation (MEEP).

2.2) Pattern Generation – create the exposure files (gds format in general) and proximity error correct using appropriate software.[30]

2.3) Pattern Exposure – load the sample into the chamber of the electron beam lithography system (LEO 1530/ Raith Elphy) and pump down. Once vacuum has been achieved, switch on the EHT supply and set to 30kV. Leave the system in this state for 1hr to allow the sample, stage and chamber to reach an equilibrium temperature. Set-up the exposure as indicated in the user-manual of your specific electron beam lithography system . Expose the sample using an appropriate basic step size (e.g. 2nm) (this being the minimum pixel size that the system can expose), a settling time of at least 1ms (this being the time the system waits between moving the beam and exposing the particular portion of the pattern), and an area dose of 55μAcm$^{-2}$.

2.4) Sample Development – using CAUTION Xylene (Xylene is both flammable and highly toxic work in a well-ventilated area away from ignition sources and avoid contact with

skin and eyes) at a temperature of 23°C develop the sample for 45s. Rinse in isopropanol.

**3.) Patten Transfer**

3.1) RIE Chamber Cleaning – Set the flow rates of argon and hydrogen to 200sccm. Throttle down the pump, via a butterfly valve, to achieve chamber pressure of $1\times10^{-1}$mBar. Set the RF power to 100W, ignite the plasma and run for at least 10min – a DC bias of approximately 700V should be observed. After switching off the $Ar/H_2$ plasma, allow the chamber to pump for approximately 1min. Set the flow rate of oxygen into the chamber to 200sccm and again throttle the chamber pressure down to $1\times10^{-1}$mBar. Ignite a second plasma of oxygen with a power of 100W and run for 5min. After these procedures, the chamber will be free of contaminants, such as polymer residues, from any previous dry etch. We perform this procedure before every change in etch recipe to ensure maximum repeatability. This procedure is optimised for our system which consists of a parallel-plate, cathode loaded, RIE; with a main chamber 12 inches in diameter by 14 inches in height, including a 12 inch port with both throttling valve and turbo-molecular pump attached.

3.2) Photonic Crystal Etching – load the sample into the RIE main chamber and pump the system down to a background pressure of $<3\times10^{-6}$mBar to ensure the chamber is free of water vapour. Begin the etch by pre-conditioning the chamber with the etching gasses (namely $CHF_3$ and $SF_6$): set the flow rate of both gasses to 100sccm (i.e. set a gas ratio of 1:1) and using the throttle bring the chamber pressure to $5\times10^{-2}$mBar; allow the gasses to flow for at least 10min. After pre-conditioning, set the RF power to approximately 20W and ignite a plasma; etch the sample for approximately 2min (the etch rate of silicon for these etch parameters is approximately 150nm/min), while ensuring that a chamber pressure of $5\times10^{-2}$mBar is maintained. A DC bias between 200-220V should be achieved throughout the etching period.

3.3) Sample Cleaning to remove remaining electron sensitive resist – after dry etching, clean the sample by rinsing in CAUTION 1165 Remover (1165 is flammable and can cause irritation to eyes, nose and respiratory tract) with ultrasonic agitation for 1-2min, followed by acetone and isopropanol as outlined above (step 1.2).

3.4) Membrane Isolation – spin-coat the sample with UV sensitive photo resist CAUTION Microposit S1818 G2 (S1818 G2 is both flammable and causes irritation to eyes, nose and respiratory tract) (see step 1.3). Using an appropriate photomask, define windows within the resist above the photonic crystal patterns using the UV mask aligner. Expose the sample for approximately 30-45s. Develop the resist in CAUTION Microposit Developer MF-319 (MF-319 is an alkaline liquid and can cause irritation to eyes, nose and respiratory tract) for 30-45s, rinsing afterwards in de-ionised water. Prepare a plastic beaker with a mixture of CAUTION 1:5 Hydrofluoric acid (1.1499g/mL 48-51% HF) (HF is extremely corrosive and readily destroys tissue, when handling use full personal protective equipment rated for HF) to de-ionised water. Note that for safety reasons only plastic beakers and tweezers should be used with Hydrofluoric acid. Submerge the sample in the Hydrofluoric acid mixture for 15min. After etching, rinse the sample thoroughly in de-ionised water. Remove the remaining photo-resist using acetone and isopropanol (see step1.2) – from this stage and onwards ultrasonic agitation cannot be used. To ensure the sample is as clean as possible, follow the acetone and isopropanol wash with a rinse in CAUTION Piranha solution

(Piranha solution is very energetic, potentially explosive and attacks organic materials, when handling use full personal protective equipment) (3:1 CAUTION sulphuric acid (sulphuric acid is corrosive and very toxic, when handling use personal protective equipment and avoid inhalation of vapours or mists) to CAUTION hydrogen peroxide (hydrogen peroxide is very hazardous in case of skin and eye contact, when handling use personal protective equipment)) for 5min, then rinse the sample in de-ionised water, acetone and isopropanol. Note that for safety reasons only glass beakers and metal tweezers should be used with the Piranha solution. As Piranha solution can explode in contact with acetone or isopropanol, it should be handled away from these reagents.

**3.5)** Facet Cleaving – if preparing a photonic crystal slow-light waveguide, the sample requires facet cleaving. Cleave the sample by following the same procedure as outlined in step 1.1, except that as small a scratch as possible should be used. An SOI chip with ~700μm thick substrate can be reliably cleaved down to 4-5mm long samples.

**4.) Photonic Crystal Slow-light Waveguide Characterisation**

4.1) Preliminary preparation of the setup – connect the output of a CAUTION broadband amplified spontaneous emission (ASE) light source (invisible IR radiation: avoid unnecessary high powers, cover beam path if possible) to a 3dB fibre splitter and use each of the outputs to couple light into the two arms of a free-space Mach-Zehnder interferometeter (MZI), as shown in Figure 9. Use aspheric lenses to collimate the light output from the fibres. In one of the arms of the interferometer, use two additional aspheric lenses to couple the light beam in and out of the sample chip. Place a polarisation beam splitter (PBS) in the sample arm to TE-polarise the light inputting the sample. Use aspheric lenses to couple the collimated output beams from both arms back into a second 3dB fibre splitter, where they will recombine. Connect one of the outputs to an infrared detector and use the reading of the detector to maximise the light coupling into the sample; connect the other output to an optical spectrum analyser (OSA). The two arms of the MZI should have approximately the same optical length when in the presence of the sample: make sure that the fibres in the two arms of the MZI have the same nominal length and include a tunable delay stage in the reference arm to allow for fine adjustment of its length. In the sample arm, mount the aspheric lenses onto *xyz* precision stages to obtain the best coupling into the sample.

4.2) Adjust reference arm length – couple the light beam to a blank (i.e. without photonic crystal) ridge waveguide (of the same type as the access waveguides that feed light inside the photonic crystals) within the same chip in the sample arm. Run a continuous scan on the OSA and observe the measured wavelength spectra. If the two arms of the MZI have approximately the same optical length, the spectra exhibit fringes due to constructive and destructive interference; these fringes will not appear if the arms of the MZI have very different optical lengths (>~cm). The fringe spacing is inversely proportional to the difference in optical path length between the two arms. Move the delay stage to make the reference arm shorter and observe the fringes in the OSA: if they become denser (sparser), the reference arm is shorter (longer) than the sample arm. Set the delay stage to make sure that the reference arm is shorter than the sample arm and results in a fringe spacing of about 5 to 10 fringes in a 10nm wavelength range (see Figure 10a). Finally, perform this optimisation on the device that provides the maximum delayg and then keep the delay fixed throughout the measurement of the entire sample.

4.3) Calibration run – while still aligned on the blank waveguide, run three scans on the OSA: one scan for the interference spectrum and one scan for each of the two arms separately (obtained by blocking the other arm). Use a resolution of 0.05-0.1nm. Record each measured spectrum.

4.4) Slow light data acquisition – run and record three spectra as in step 4.3 for each photonic crystal waveguide on the chip.

4.5) Fourier data analysis – the interference spectrum (interferogram) $I(\omega)$ is mathematically expressed by:

$$I(\omega) = S(\omega) + R(\omega) + \mathrm{sqrt}[S(\omega)R(\omega)]\{\exp[i\Phi(\omega) - i\omega\tau] + \mathrm{c.c.}\},$$

where $S(\omega)$ and $R(\omega)$ are the spectral densities measured separately from the sample and reference arms, respectively. The delay $\tau$ is set by the position of the delay stage in the reference arm. The information on the dispersion of the photonic crystal waveguide is contained in the phase term, which we must extract from the measured data.

Subtract the non-interfering background $S(\omega)+R(\omega)$ from the interferogram to isolate only the interfering term. Calculate the Fourier transform of the interfering term: the term $\mathrm{sqrt}(SR)\exp[i(\Phi- \omega\tau)]$ and its complex conjugate correspond to peaks centred at $t=\tau$ and $t=-\tau$, respectively. Filter numerically one of the two terms and transform back to the frequency domain. Differentiate the phase $\Phi(\omega) - \omega\tau$ of the resulting data with respect to $\omega$ to obtain $\Delta\tau_g$, the difference in group delay between the two arms. The group index $n_g=c/v_g$, with $v_g$ the group velocity, is given by:

$$n_g = (\Delta\tau_g^{PhC} - \Delta\tau_g^{cal})c/L + n_{cal},$$

where $\Delta\tau_g^{cal}$ is obtained from the calibration data taken from the blank waveguide, $L$ is the photonic crystal waveguide length and $n_{cal}=2.7$ is the effective index of the reference ridge waveguide. The contribution to the delay from the various optical elements of the setup is taken into account in the calibration run, and is therefore subtracted in this step.

4.6) Transmission curve – calculate the transmission curve by normalising the sample spectrum of a photonic crystal waveguide to that of the blank waveguide.

**5.) Photonic Crystal Cavity Characterisation**

5.1) Setup – the preparation of the setup (Figure 14) for RS includes: switching of the exchangeable element to the polarising beam splitter; inserting a polariser in the input arm as well as an analyser in the output arm; flip a mirror into the probe arm to allow the use of a near-infrared source; allow the illumination of the sample. Mount the sample vertically with a 45º orientation to axis of the polarizer (Figure 18) on a differential driven *xyz* micro-block and adjust the micro-block so that the sample is in focus and a cavity can be seen with the camera, as in Figure 15 (left). Using an amplified spontaneous emission (ASE) source, align the beam with the centre of the cavity Figure 15 (right). Flip away the illumination mirror and allow the output arm to enter the spectrometer (monochromator with attached array detector). Start a broad scan with a low to moderate resolution in order to identify the cavity peaks. Obtain the coarse wavelength of the resonance in the ASE scan (Figure 16a) with an accuracy of

±1nm. It is also possible to acquire the broad scan with a CAUTION tunable laser source (TLS) (Figure 16b) (invisible IR radiation: avoid unnecessary high powers, cover beam path if possible). One has to be careful that the resolution is set to the highest value in order to sample the line-widths of every peak.

5.2) Perform high-resolution scans on the identified peaks – connect the TLS to the input arm and attenuate the beam to a μW level. Prepare for the high resolution scan by allowing the output arm to be collected by the photodetector and setting up a continuous sweep scan with a resolution of 1pm for a 2nm range centred at the previously found resonance wavelength. The importance of this step is to improve the signal-to-noise ratio (SNR) with the aim to obtain a Lorentzian line-shape resonance: change the *xyz* position of the micro-block and re-run the scan until the SNR is maximised and the line-shape is close to that of a Lorentzian, as shown in the representative result section.

**Representative Results:**

**Fabricated samples:**

**Figure 1** shows a scanning electron microscope (SEM) image of an exposed and developed pattern in electron beam resist – it is evident from the "clean" edge between the resist and the silicon substrate that complete exposure/development has been accomplished. Exposure of dose test patterns, consisting of simple repeated shapes (in our case 50×50μm squares), each with a differing base dose, are used to determine the correct dose factor and development time for subsequent films.

When creating high resolution features using electron beam lithography, it is beneficial to use as thin a film of resist as possible; when etching the features into silicon, however, it is advisable to use the thickest possible film. Balancing these opposing conditions is the goal of optimising the fabrication recipe: we have found that a layer of ZEP 520A approximately 350nm thick gives the required high-resolution while still withstanding the etching process.

**Figure 2** shows an SEM image of a second sample which has been exposed, developed and etched using the reactive ion etching (RIE) system: the sample shows vertical sidewalls in each photonic crystal hole and no widening of the holes at either surface of the silicon. **Figure 3** is of a completed membrane photonic crystal device: the hydrofluoric etch is somewhat isotropic, in that it etches the silica layer nearly equally in every direction. A relatively tight control of the under-etch must therefore be maintained, or too long an etch will cause the photonic crystal membranes to collapse.

In **Figure 4** we present a close-up image of an optimised photonic crystal etch: the vertical sidewalls, the lack of striations and edge-wall roughness are clear to see. This etch was performed using the following parameters: etch pressure 5 x $10^{-2}$mBar, etch time 1min 40s, RF power 19W producing a DC bias of -210V, and 50:50 gas ratio of $SF_6$ and $CHF_3$.

Increasing the RIE etching pressure above optimum (i.e. to 5.9 x $10^{-2}$mBar, an increase of 18%) introduces an angle in the photonic crystal wall, as can be seen in **Figure 5**. This effect becomes more prevalent as the pressure is increased further. On the other hand, increasing the RF power, which results in a larger DC bias (i.e. RF power of 22W resulting in a DC bias of -232V, increases of 15% and 10% respectively), causes a faster break-down of the etch

mask producing a widening of the top of the photonic crystal holes, as can be seen in **Figure 6**. **Figure 7** shows the result of over-etching a photonic crystal, the longer etch time (i.e. 2min 20s, 40% increment) allowing the resist to completely break down resulting in the widening of the photonic crystal holes – creating both of the above effects i.e. photonic crystal hole widening and angled sidewalls. Finally, in **Figure 8** we see the results of poor optimisation of both etch pressure and time: this micrograph indicates that the etch mask has started to break-down causing striations in the photonic crystal holes.

Each of these effects, if not corrected, manifests itself as a higher propagation loss in the final device: propagation losses may arise from both a high density of scattering centres (especially observed in devices with high side-wall roughness) and from a break in symmetry of the photonic crystal structure (as seen in non-verticality and hole widening).[31-32]

**Measured slow light group index curves:**
A typical example interferogram measured from a blank waveguide is shown in **Figure 10a**. The raw measured data is shown in grey, and is affected by strong Fabry-Perot fringes that result from the high reflectivity at the facets of the waveguide. For clarity, we have numerically filtered out the Fabry-Perot fringes, as shown in the black curve. The fringes resulting from the interference of the sample and reference arms of the MZI setup are clearly visible, and they are uniformly distributed over the entire wavelength range.

The interferogram from an 80μm long engineered slow light photonic crystal waveguide on the same chip is shown in **Figure 10b**: the fringes become denser at wavelengths higher than 1575nm, marking the transition from the fast to the slow light regime. Note that an increase of the group index, corresponding to an increase of the sample arm optical length, will always result in a monotonic reduction of the fringe spacing, as we have deliberately set the delay stage to make sure the reference arm is the shortest.

The corresponding group index curve is shown in **Figure 11** (blue curve): from a value of around 5 in the fast light regime, it increases to around 46, where it remains constant over a bandwidth of ~6nm. The group index curve shown here has been smoothened from the Fabry-Perot noise by performing a running average on the phase term just before differentiation. Note from **Figure 10b** that past the cutoff, where the photonic crystal does not transmit light, there are no fringes, and therefore any resulting group index data at these wavelengths is a measurement artefact.

The transmission curve calculated as the ratio between the transmission of the photonic crystal waveguide and the blank waveguide is also shown as the black line in **Figure 11**, with a sharp cutoff clearly visible around 1594nm.

**Figures 12 and 13** illustrate the capability of our measuring technique: **Figure 12** shows measured group indices in excess of 100 for an 80μm long waveguide, and **Figure 13** shows a measured group index of almost 90 for a 300μm long waveguide. These waveguides were fabricated on the same chip as the waveguides of **Figures 10-11**. The pronounced dips appearing in the transmission curve when approaching the mode cutoff are believed to the signature of multiple scattering.[33]

**Cavities:**
In order to obtain the resonant wavelength and the *Q*-factor, the line-shape from the high-resolution scan needs to be fitted. As the coupling to the cavity is governed by Fano resonances, we use the following Fano-function to obtain a proper fit of the line-shape:[14]

$$Y = y_0 + A*((q+2*(\lambda-\lambda_0)/\Delta\lambda)^2/(1+(2*(\lambda-\lambda_0)/\Delta\lambda))^2),$$

where $y_0$ is an offset, $A$ an area constant, $q$ a dimensionless parameter that gives the ratio between the resonant and non-resonant amplitudes, $\lambda_0$ is the resonant wavelength and $\Delta\lambda$ is the full-width half-maximum (FWHM) of the resonance.

In general, the fitting is easier the closer the line-shape is to that of a Lorentzian because, in the first fitting steps, $q$ can be fixed at 0 and $\lambda_0$ to the centre of the peak. An example of such a Lorentzian line-shape with a high SNR is shown in **Figure 17a**. The wavelength is determined as 1562.162nm and $q$ is -0.0891. The *Q*-factor is calculated according to:

$$Q = \lambda_0/\Delta\lambda,$$

so that *Q* results in 41,382. In the case that no Lorentizan line-shape can be obtained during the measurement steps in 5.2, the fit is still possible but more difficult, due to more unknown fitting parameters. For example, in **Figure 17b** the peak of the line-shape does not correspond to the resonant wavelength, indicated by the dashed line. The *Q*-factor, however, is close to that obtained in **Figure 17a**. If the SNR is low, the fitting error obviously increases, and a Lorentzian line-shape (**Figure 17c**) gives a more accurate *Q*-factor than an asymmetric Fano line-shape (**Figure 17d**).

**Tables and Figures:**

**Figure 1:** Photonic crystal pattern in electron beam resist (ZEP520A).

**Figure 2:** Photonic crystal pattern after etching, in silicon.

**Figure 3:** Photonic crystal waveguide after undercut etch with hydrofluoric acid.

**Figure 4:** Photonic crystal in silicon etched with optimised RIE recipe. Of note are the straight vertical side walls and the little to no side-wall roughness.

**Figure 5:** Photonic crystal etched with increased RIE chamber pressure. Angled side-walls are evident.

**Figure 6:** Photonic crystal etched with higher RF power (and DC bias). Holes show evidence of widening at surface.

**Figure 7:** Over etched photonic crystal. Angled side-walls due to resist breakdown and overall widening of holes evident.

**Figure 8:** Poorly optimised etch (i.e. both pressure and time). Mask break-down has caused striations at the top of each hole.

**Figure 9:** Schematic of the Mach-Zehnder interferometric setup used to measure transmission and group index curves of slow light photonic crystal waveguides.

**Figure 10:** Measured interferograms of (a) a blank ridge waveguide and (b) an 80μm long engineered slow light photonic crystal waveguide on the same chip. The original data is shown as the grey curve in the background. The black curve has been numerically filtered to remove Fabry-Perot fringes.

**Figure 11:** Group index (blue) and transmission (black, grey) curves of the same waveguide as in Figure 10(b). The transmission curve is obtained by normalising to that of the blank ridge waveguide. The black curve has been numerically filtered to remove Fabry-Perot fringes.

**Figure 12:** Group index (blue) and transmission (black, grey) curves of an 80μm long waveguide. The transmission curve is obtained by normalising to that of a blank ridge waveguide on the same chip. The black curve has been numerically filtered to remove Fabry-Perot fringes.

**Figure 13:** Group index (blue) and transmission (black, grey) curves of a 300μm long waveguide. The transmission curve is obtained by normalising to that of a blank ridge waveguide on the same chip. The black curve has been numerically filtered to remove Fabry-Perot fringes.

**Figure 14:** Top-view of multi-functional characterisation setup with exchangeable element. The probe beam from the input arm (green) is centred at the high NA objective that focuses it on the mounted sample. Alignment to the centre is obtained by illuminating the cavity with a light source (yellow) and visualising the cavity with the camera. The signal form the output arm (red) can then be directed to a free-space spectrometer or a fibre coupled detector.

**Figure 15:** Captured image as appears on screen with beam off (left) and on (right). The beam is clearly aligned with the centre of the cavity.

**Figure 16:** Initial broadband scan to identify the cavity resonances. In both the ASE (a) and the TLS (b) scans a strong resonance is visible above 1560nm.

**Figure 17:** High-resolution scans with the TLS. (a) Lorentzian line-shape high SNR. (b) Near Lorentzian line-shape with high SNR. (c) Lorentzian line-shape with low SNR. (d) Asymmetric Fano line-shape with low SNR. The dashed lines indicate the resonance wavelength.

**Figure 18:** Arrangement of polarising optics (a) to the sample (b) (from Reference [29]). The polariser orientates the polarisation in *x*-direction and the beam splitter only reflects *y*-polarised light, with the analyser further increasing the SNR of *y*- to *x*-polarised light at the output arm. 

**Discussion:**

**Sample fabrication:**

Our choice of electron-beam resist (i.e. ZEP 520A) is due to its simultaneously high resolution and etch resistance. Finally, we believe that ZEP 520A may be affected by the UV light emitted from overhead laboratory lights; as such we recommend placing spin-coated samples in UV opaque containers while moving them from one laboratory to another.

Moving onto defining the photonic crystal pattern, before exposing the sample we have found that allowing the electron beam lithography system to settle for at least an hour after loading reduces mis-alignment errors during writing – this is due to the sample stage and vacuum chamber not being at the same temperature immediately after loading. As photonic crystal patterns, along with access waveguides, may take several hours to write, a small drift in the stage relative to the chamber (even at only nanometres per photonic crystal hole) results in significant stitching and possibly pattern distortion errors with respect to photonic crystal tolerances. This error is random in nature, from one exposure to another, but can be as high as 100 nm/min (absolute positional error), however relative positional error i.e. between one photonic crystal hole to another can be on the order of nanometres, which can be further reduced by increasing the speed at which the pattern is written. As mentioned these issues can be further negated (although never completely removed) by allowing the system to settle after first loading the sample.

The $Ar/H_2$ plasma etch (used to remove metal and silicon contaminants through ion bombardment) followed by $O_2$ plasma etch (used for the removal of polymer and organic residue through plasma ashing) described in section 3.1 of the protocol define a cleaning regimen that was developed to control contamination within the RIE chamber when etching the photonic crystals – this cleaning is considered, by us to be one of the most important steps in the fabrication of photonic crystal devices, cleaning of the RIE chamber is paramount to repeatable reliable fabrication especially as in our case where the RIE is not used solely for the etching of silicon. The $Ar/H_2$ plasma is seen to change from a blue-grey colour (indicating a contaminated chamber) to a pink colour (indicating that the chamber is free of contaminants); a 10min plasma is normally sufficient. The $O_2$ plasma is then carried out for a further 5-10min depending on the cleanliness of the chamber at the beginning of the process (i.e. $Ar/H_2$ plasma colour). Although the previous method has not be conclusively proven we find that the colour of the plasma proves a useful indicator for chamber cleanliness. We have also found that by pre-conditioning the etch chamber with the silicon etch gasses for 10min results in a more reliable process – we believe this to be due to the etching gas flow rates stabilising and being adsorbed into the chamber walls during the pre-condition period.

When under-etching the sample, to create membranes, using hydrofluoric acid, the access waveguides must be protected. If the hydrofluoric acid comes into contact with the access waveguide, it penetrates through the now etched trench (either side of the waveguide) and under-etches the access waveguides for hundreds of micrometres. In extreme cases the access waveguides may bend and break due to stresses, rendering a complete chip useless. As hydrofluoric acid is an isotropic etchant, the etching time must be controlled to prevent lateral etching (perpendicular to the photonic crystal waveguide) from causing the membrane to bend due to release of the stress intrinsic to the silicon layer. In extreme cases, the excessive under-etch can also cause the membrane to collapse.

Finally, the creation of clean facets for the free-space coupling of light into photonic crystal waveguides is extremely challenging. If scratched/cleaved carefully, silicon will essentially follow a crystal plane forming a good facet (in our experience, techniques such as facet polishing are not required). A bad facet can cause large coupling losses at each facet. We recommend perfecting a cleaving technique before attempting to work with important samples. It is equally imperative that once a good cleave has been achieved the facets are not damaged: the sample should only be lifted using the two edges parallel to the waveguides (i.e. not by the end facet sides of the chip). Sample lengths down to 2-3mm can be reliably achieved with manual cleaving of a ~700μm thick SOI chip. For smaller samples, we suggest thinning the substrate or use a different cleaving technique.

Although the protocol outlined in this paper is optimised for SOI, the general principle behind the fabrication methods are also valid for the fabrication of devices into other semiconductors, of course when changing from silicon careful consideration of etch-tool, etch-chemistries and mask materials would need to be made.

The fabrication protocol of this paper is optimised for devices targeted at an operating centre wavelength of 1550nm, however devices have also been prepared for the MidIR (2.7-3.5μm) regime using fabrication protocols based on the ones presented in this paper.

**Slow light group index measurements:**

The significance of the group index as the key parameter to measure slow light originates from the dispersion diagram or band structure $\omega(k)$ typically used to describe the dispersion of a photonic crystal waveguide.[34] The local slope of the dispersion curve $\partial\omega/\partial k$ corresponds to the group velocity $v_g$, i.e. the speed at which the electromagnetic energy travels through the waveguide, which can be equivalently described by the group index $n_g=c/v_g$. Values of $n_g$ around 5 correspond to the fast light regime, whereas higher values are typically considered to fall within in the slow light regime.

When building the slow light MZI setup, it is important to make sure that all the fibres of the two arms of the interferometer are securely tied to the optical table, as any movement or vibration will change the path lengths compromising the quality of the interferogram acquisition. For the same reason, the scan of the interferogram should be performed quickly, or fluctuations of the phase will result in unwanted oscillations of the group index data. The two arms of the MZI may also be realised entirely in free space to avoid fibres altogether, as in Reference [26]: a free-space MZI will be more stable, but also more difficult to align.

Depending on the resolution set and the strength of the Fabry-Perot fringes, the determination of the group index is affected by large uncertainty when the fringes converge very tightly. Setting the delay stage to initially give 4-10fringes/10nm, as detailed in step 4.2 of the protocol, works well for photonic crystal waveguides of lengths 30-100μm with relatively high group indices, up to $n_g$>100 for engineered slow light waveguides[35] (see **Figure 12**). For band-edge slow light, the maximum measurable group indices tend to be lower for the same length, due to the higher propagation losses.

With a fringe spacing of ~4fringes/10nm we are able to reliably measure group indices up to almost 100 also in 300μm long engineered waveguides (**Figure 13**). For longer waveguides, the fringes become very dense very quickly, and the resolution of the OSA will limit the maximum measurable group index. Note, however, that for a fixed resolution and fringe

spacing, the maximum measurable group index does not scale linearly with waveguide length, and may also be influenced by propagation loss dispersion. For a very long waveguide, we suggest to include next to it a short waveguide with identical design specifically for group index measurement.

In summary, we have described a simple and powerful method for the experimental determination of the dispersion properties of slow light photonic crystal waveguides. Our technique is based on the combination of frequency domain interferometry[23] with Fourier transform analysis[36] and allows for a direct, single-shot, continuous mapping of the group index curve, with no need for delay scans,[23-24] nonlinear fitting of data[22,25] or determination of the position of fringe extrema.[20-21,25] By using a broadband light source, we are able to extract information from the sample over a large wavelength range, and in a very stable and repeatable manner. We can measure group indices in excess of 100 for both short and moderately long waveguides (up to 200-250μm), which are values much higher than those needed for the useful application of slow light waveguides for enhancing the performance of both linear and nonlinear devices.

**Resonant scattering:**

Photonic crystal cavities confine light in-plane in two dimensions, in contrast to photonic crystal waveguides, where light is guided in one dimension. This allows the storage of light within ultra-small volumes, which is described by an energy decay, analogue to i.e. that of an electronic resonator. In photonic systems, this decay is associated with the photon lifetime of the cavity and is of exponential form, hence resulting in a Lorentzian lineshape of the peak. The ratio of the peak centre wavelength to the Full-Width Half-Maximum represents the *Q*-factor.

An important feature of the RS technique is the polarisation maintaining property of the setup and especially that of the high NA objective. Here lies the issue with the compatibility of having a high NA (high collection efficiency) while maintaining the polarisation, because high NA objectives tend to mix polarisations. This polarisation intermixing is responsible for small peaks and low SNR.

When the off-resonance, *x*-polarised light arrives at the cavity (**Figure 18a**), it is back scattered through the objective and filtered out by the beam splitter/analyser (*y*-polarised), so that only a low level is seen at the detector. In the case of polarisation intermixing, some of the *x*-polarised light is converted to the opposite polarisation and can pass the analyser thus increasing the background. If then on-resonance light couples to the cavity, the polarisation rotates for the fundamental cavity mode (red arrow in **Figure 18b**) and creates a *y*-polarisation component. This light is directed to the output arm and passes the analyser. Again, the *y*-polarised light can convert to the opposite polarisation thus reducing the signal level. Therefore, an objective needs to be chosen so that polarisation intermixing is kept at a minimum.

For ultra-high *Q*-factor cavities, such as a hetero-structure cavity, the emitted power is lower. This situation can further reduce the SNR and the peak vanishes in the noise level. A lock-in configuration should then be used to lower the noise level, not the background level, in order to recover the peak.

Note that our setup (**Figure 14**) is designed for multi-functional cavity characterisation, and in addition to RS includes micro-photoluminescence and the generation of second and third harmonic frequencies.

**Acknowledgments:**
The authors gratefully acknowledge Dr Matteo Galli, Dr Simone L. Portalupi and Prof. Lucio C. Andreani from the University of Pavia for helpful discussions related to the RS technique and the execution of measurements.

**Disclosures:**
The authors have nothing to disclose.

**Reagents:**

| Name | Company | Catalogue number | Comments (optional) |
|---|---|---|---|
| Acetone | Fisher Scientific | A/0520/17 | CAUTION: flammable, use good ventilation and avoid all ignition sources |
| Isopropanol | Fisher Scientific | P/7500/15 | CAUTION: flammable, use good ventilation and avoid all ignition sources |
| Electron Beam resist | Marubeni Europe plc. | ZEP520A | CAUTION: flammable, harmful by inhalation, avoid contact with skin and eyes |
| Xylene | Fisher Scientific | X/0100/17 | CAUTION: flammable and highly toxic, use good ventilation, avoid all ignition sources, avoid contact with skin and eyes |
| Microposit S1818 G2 | Chestech Ltd. | 10277866 | CAUTION: flammable and causes irritation to eyes, nose and respiratory tract |
| Microposit Developer MF-319 | Chestech Ltd. | 10058721 | CAUTION: alkaline liquid and can cause irritation to eyes, nose and respiratory tract |
| Hydrofluoric Acid | Fisher Scientific | 22333-5000 | CAUTION: extremely corrosive, readily destroys tissue; handle with full personal protective equipment rated for HF |
| Microposit 1165 Remover | Chestech Ltd. | 10058734 | CAUTION: flammable and causes irritation to eyes, nose and respiratory tract |
| Sulphuric Acid | Fisher Scientific | S/9120/PB17 | CAUTION: corrosive and very toxic; handle with personal protective equipment and avoid inhalation of vapours or mists |
| Hydrogen Peroxide | Fisher Scientific | BPE2633-500 | CAUTION: very hazardous in case of skin and eye contact; handle with personal protective equipment |

**Equipment:**

| Name | Company | Catalogue number | Comments (optional) |
|---|---|---|---|
| Silicon-on-Insulator wafer | Soitec | G8P-110-01 | |
| Diamond Scribe | J & M Diamond Tool Inc. | HS-415 | |
| Microscope slides | Fisher Scientific | FB58622 | |
| Beakers | Fisher Scientific | FB33109 | |
| Tweezers | SPI Supplies | PT006-AB | |
| Ultrasonic Bath | Camlab | 1161436 | |

| | | | |
|---|---|---|---|
| Spin-Coater | Electronic Micro Systems Ltd. | EMS 4000 | |
| Pipette | Fisher Scientific | FB55343 | |
| E-beam Lithography System | Raith Gmbh | Raith 150 | |
| Reactive Ion Etching System | Proprietary In-house Designed | -- | |
| UV Mask Aligner | Karl Suss | MJB-3 | |
| ASE source | Amonics | ALS-CL-15-B-FA | CAUTION: invisible IR radiation |
| Single mode fibres | Thorlabs | P1-SMF28E-FC-2 | |
| 3dB fibre splitters | Thorlabs | C-WD-AL-50-H-2210-35-FC/FC | |
| Aspheric lenses | New Focus | 5720-C | |
| XYZ stages | Melles Griot | 17AMB003/MD | |
| Polarising beamsplitter cube | Thorlabs | PBS104 | |
| IR detector | New Focus | 2033 | |
| 100×Objective | Nikon | BD Plan 100x | |
| Oscilloscope | Tektronix | TDS1001B | |
| Optical Spectrum Analyser | Advantest | Q8384 | |
| IR sensor card | Newport | F-IRC2 | |
| TLS source | Agilent | 81940A | CAUTION: invisible IR radiation |
| IR Camera | Electrophysics | 7290A | |
| IR Detector | New Focus | 2153 | |
| Digital Multimeter | Agilent | 34401A | |
| Illumination | Stocker Yale | Lite Mite | |
| Monochromator | Spectral Products | DK480 | |
| Array Detector | Andor | DU490A-1.7 | |
| GIF Fibre | Thorlabs | 31L02 | |

## References:


1. Baba, T., Kawasaki, T., Sasaki, H., Adachi, J. & Mori, D. Large delay-bandwidth product and tuning of slow light pulse in photonic crystal coupled waveguide. *Opt. Express* **16** (12), 9245-9253, doi:10.1364/OE.16.009245 (2008).
2. Melloni, A., Canciamilla, A., *et al.* Tunable delay lines in silicon photonics: coupled resonators and photonic crystals, a comparison. *IEEE Photon. J.* **2** (2), 181-194, doi:10.1109/JPHOT.2010.2044989 (2010).
3. Ishikura, N., Baba, T., Kuramochi, E. & Notomi, M. Large tunable fractional delay of slow light pulse and its application to fast optical correlator. *Opt. Express* **19** (24), 24102-24108, doi:10.1364/OE.19.024102 (2011).
4. Beggs, D. M., Rey, I. H., Kampfrath, T., Rotenberg, N., Kuipers, L. & Krauss, T. F. Ultrafast tunable optical delay line based on indirect photonic transitions. *Phys. Rev. Lett.* **108** (21), 213901, doi:10.1103/PhysRevLett.108.213901 (2012).
5. Beggs, D. M., White, T. P., O'Faolain, L. & Krauss, T. F. Ultracompact and low-power optical switch based on silicon photonic crystals. *Opt. Lett.* **33** (2), 147-149, doi:10.1364/OL.33.000147 (2008).

6. Nguyen, H. C., Sakai, Y., Shinkawa, M., Ishikura, N. & Baba, T. 10Gb/s operation of photonic crystal silicon optical modulators. *Opt. Express* **19** (14), 13000-13007, doi:10.1364/OE.19.013000 (2011).
7. Kampfrath, T., Beggs, D. M., White, T. P., Melloni, A., Krauss, T. F. & Kuipers, L. Ultrafast adiabatic manipulation of slow light in a photonic crystal. *Phys. Rev. A* **81** (4), 043837, doi:10.1103/PhysRevA.81.043837 (2010).
8. Monat, C., Corcoran, B. *et al.* Slow light enhancement of nonlinear effects in silicon engineered photonic crystal waveguides. *Opt. Express* **17** (4), 2944-2953, doi:10.1364/OE.17.002944 (2009).
9. Corcoran, B., Monat, C. *et al.* Green light emission in silicon through slow-light enhanced third-harmonic generation in photonic-crystal waveguides. *Nature Photon.* **3**, 206-210, doi:10.1038/nphoton.2009.28 (2009).
10. Li, J., O'Faolain, L., Rey, I. H. & Krauss, T. F. Four-wave mixing in photonic crystal waveguides: slow light enhancement and limitations. *Opt. Express* **19** (5), 4458-4463, doi:10.1364/OE.19.004458 (2010).
11. Checoury, X., Han, Z. & Boucaud, P. Stimulated Raman scattering in silicon photonic crystal waveguides under continuous excitation. *Phys. Rev. B* **82** (4), 041308, doi:10.1103/PhysRevB.82.041308 (2010).
12. Nomura, M., Kumagai, N., Iwamoto, S., Ota, Y. & Arakawa. Y. Photonic crystal nanocavity laser with a single quantum dot gain. *Opt. Express* **17** (18), 15975-15982, doi:10.1364/OE.17.015975 (2009).
13. Ellis, B., Mayer, M. A. *et al.* Ultralow-threshold electrically pumped quantum-dot photonic-crystal nanocavity laser. *Nature Photon.* **24**, 297-300, doi:10.1038/nphoton.2011.51 (2011).
14. Galli, M., Gerace, D. *et al.* Low-power continuous-wave generation of visible harmonics in silicon photonic crystal nanocavities. *Opt. Express* **18** (25), 26613-26624, doi:10.1364/OE.18.026613 (2010).
15. Notomi, M., Shinya, A., Mitsugi, S., Kira, G., Kuramochi, E. & Tanabe, T. Optical bistable switching action of Si high-Q photonic-crystal nanocavities. *Opt. Express* **13** (7), 2678-2687, doi:10.1364/OPEX.13.002678 (2005).
16. Shambat, G., Rivoire, K., Lu, J., Hatami, F. & Vučković, J. Tunable-wavelength second harmonic generation from GaP photonic crystal cavities coupled to fiber tapers. *Opt. Express* **18** (12), 12176-12184, doi:10.1364/OE.18.012176 (2010).
17. Fan, S., Villeneuve, P. R., Joannopoulos, J. D. & Haus, H. A. Channel drop filters in photonic crystals. *Opt. Express* **3** (1), 4-11, doi:10.1364/OE.3.000004 (1998).
18. Tanabe, T., Nishiguchi, K., Kuramochi, E. & Notomi, M., Low power and fast electro-optic silicon modulator with lateral p-i-n embedded photonic crystal nanocavity. *Opt. Express* **17** (25)**,** 22505-22513, doi:10.1364/OE.17.022505 (2009).
19. Nozaki, K., Tanabe, T. *et al.* Sub-femtojoule all-optical switching using a photonic-crystal nanocavity. *Nature Photon.* **4**, 477-483, doi:10.1038/nphoton.2010.89 (2010).
20. Notomi, M., Yamada, K., Shinya, A., Takahashi, J., Takahashi, C. & Yokohama, I. Extremely large group-velocity dispersion of line-defect waveguides in photonic crystal slabs. *Phys. Rev. Lett.* **87** (25), 253902, doi:10.1103/PhysRevLett.87.253902 (2001).
21. Labilloy, D., Benisty, H., Weisbuch, C., Smith, C. J. M., Krauss, T. F., Houdré, R. & Oesterle, U. Finely resolved transmission spectra and band structure of two-dimensional photonic crystals using emission from InAs quantum dots. *Phys. Rev. B* **59** (3), 1649-1652, doi:10.1103/PhysRevB.59.1649 (1999).

22. Inanç Tarhan, I., Zinkin, M. P. & Watson, G. H. Interferometric technique for the measurement of photonic band structure in colloidal crystals. *Opt. Lett.* **20** (14), 1571-1573, doi:10.1364/OL.20.001571 (1995).
23. Galli, M., Marabelli, F. & Guizzetti, G. Direct measurement of refractive-index dispersion of transparent media by white-light interferometry. *Appl. Opt.* **42** (19), 3910-3914, doi:10.1364/AO.42.003910 (2003).
24. Galli, M., Bajoni, D., Marabelli, F., Andreani, L. C., and Pavesi, L. & Pucker, G. Photonic bands and group-velocity dispersion in $Si/SiO_2$ photonic crystals from white-light interferometry. *Phys. Rev. B* **69** (11), 115107, doi:10.1103/PhysRevB.69.115107 (2004).
25. Vlasov, Y. A., O'Boyle, M., Hamann, H. F. & McNab, S. J. Active control of slow light on a chip with photonic crystal waveguides. *Nature* **438**, 65-69, doi:10.1038/nature04210 (2005).
26. Gomez-Iglesias, A., O'Brien, D., O'Faolain, L., Miller, A. & Krauss, T. F. Direct measurement of the group index of photonic crystal waveguide via Fourier transform spectral interferometry. *Appl. Phys. Lett.* **90** (26), 261107, doi:10.1063/1.2752761 (2007).
27. Akahane, Y., Asano, T., Song, B-S. & Noda, S. High-Q photonic nanocavity in a two-dimensional photonic crystal. *Nature* **425**, 944-947, doi:10.1038/nature02063 (2003).
28. McCutcheon, M. W., Rieger, G. W. *et al.* Resonant scattering and second-harmonic spectroscopy of planar photonic crystal microcavities. *Appl. Phys. Lett.* **87** (22), 221110, doi:10.1063/1.2137898 (2005).
29. Galli, M., Portalupi, S. L., Belotti, M., Andreani, L. C., O'Faolain, L. & Krauss, T. F. Light scattering and Fano resonances in high-Q photonic crystal nanocavities. *Appl. Phys. Lett.* **94** (7), 71101, doi:10.1063/1.3080683 (2009).
30. Wüest, R., Strasser, P., Jungo, M., Robin, F., Erni, D. & Jäckel, H. An efficient proximity-effect correction method for electron-beam patterning of photonic-crystal devices. *Microelectron. Eng.* **67-68**, 182-188, doi:10.1016/S0167-9317(03)00070-4 (2003).
31. Tanaka, Y., Asano, T., Akahane, Y., Song, B.-S. & Noda., S. Theoretical investigation of a two-dimensional photonic crystal slab with truncated cone air holes. *Appl. Phys. Lett.* **82** (11), 1661, doi:10.1063/1.1559947 (2003).
32. Asano, T., Song, B.-S. & Noda, S. Analysis of the experimental Q factors (~ 1 million) of photonic crystal nanocavities. *Opt. Express* **14** (5), 1996-2002, doi10.1364/OE.14.001996 (2006).
33. O'Faolain, L., Schulz, S. A. *et al.* Loss engineered slow light waveguides. *Opt. Express* **18** (26), 27627-27638, doi:10.1364/OE.18.027627 (2010).
34. Joannopoulos, J. D., Johnson, S. G., Winn, J. N. & Meade, R. D. Photonic crystals, molding the flow of light. Princeton University Press, 2nd ed., 2008.
35. Li, J., White, T. P., O'Faolain, L., Gomez-Iglesias, A. & Krauss, T. F. Systematic design of flat band slow light in photonic crystal waveguides. *Opt. Express* **16** (9), 6227-6232, doi:10.1364/OE.16.006227 (2008).
36. Takeda, M., Ina, H. & Kobayashi, S. Fourier-transform method of fringe-pattern analysis for computer-based topography and interferometry. *J. Opt. Soc. Am.* **72** (1), 156-160, doi:10.1364/JOSA.72.000156 (1982).

Figure 1: Photonic crystal pattern in electron beam resist (ZEP5
Click here to download Figure: Fig01.eps

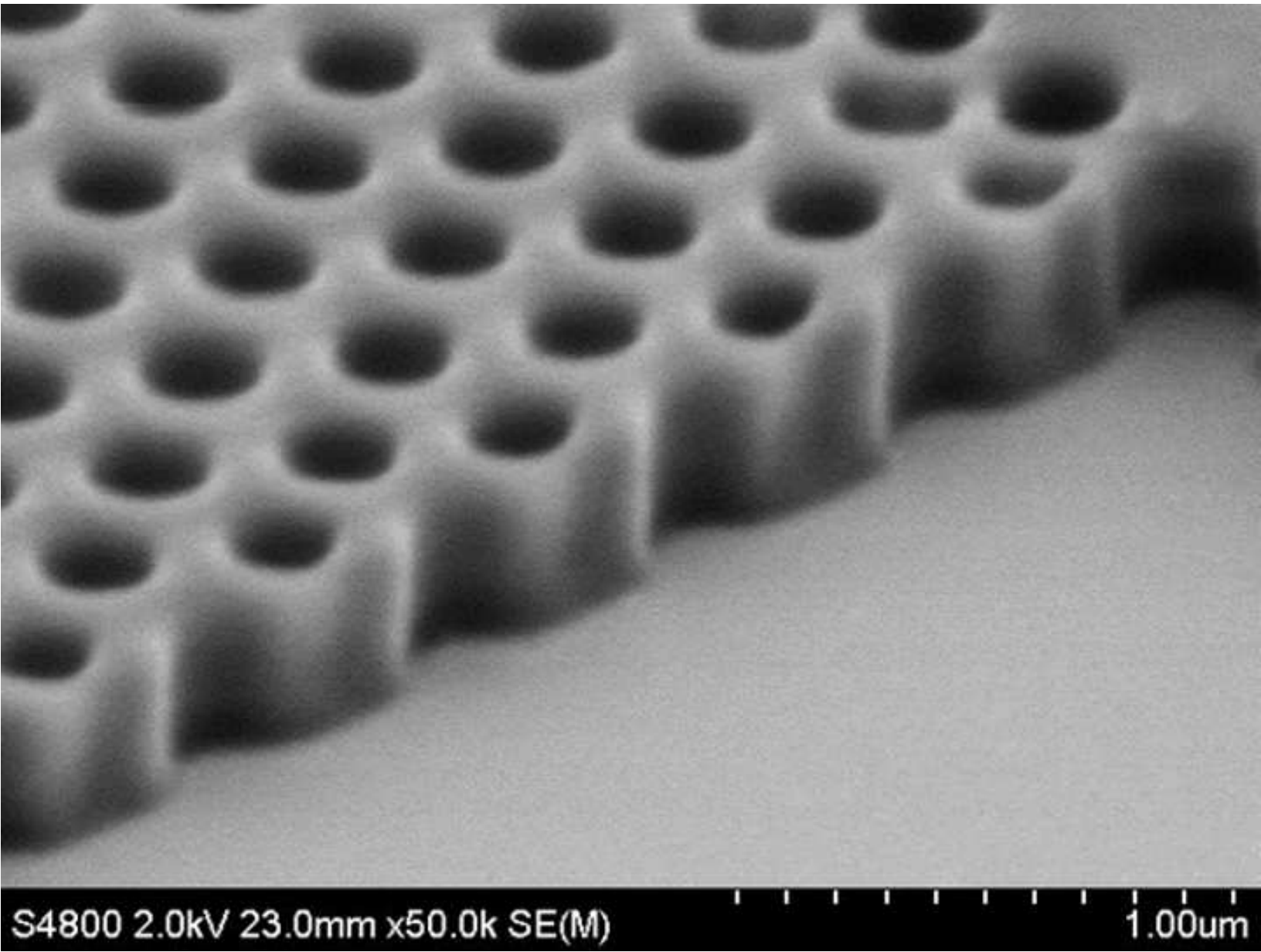

Figure 2: Photonic crystal pattern after etching, in silicon.
Click here to download Figure: Fig02.eps

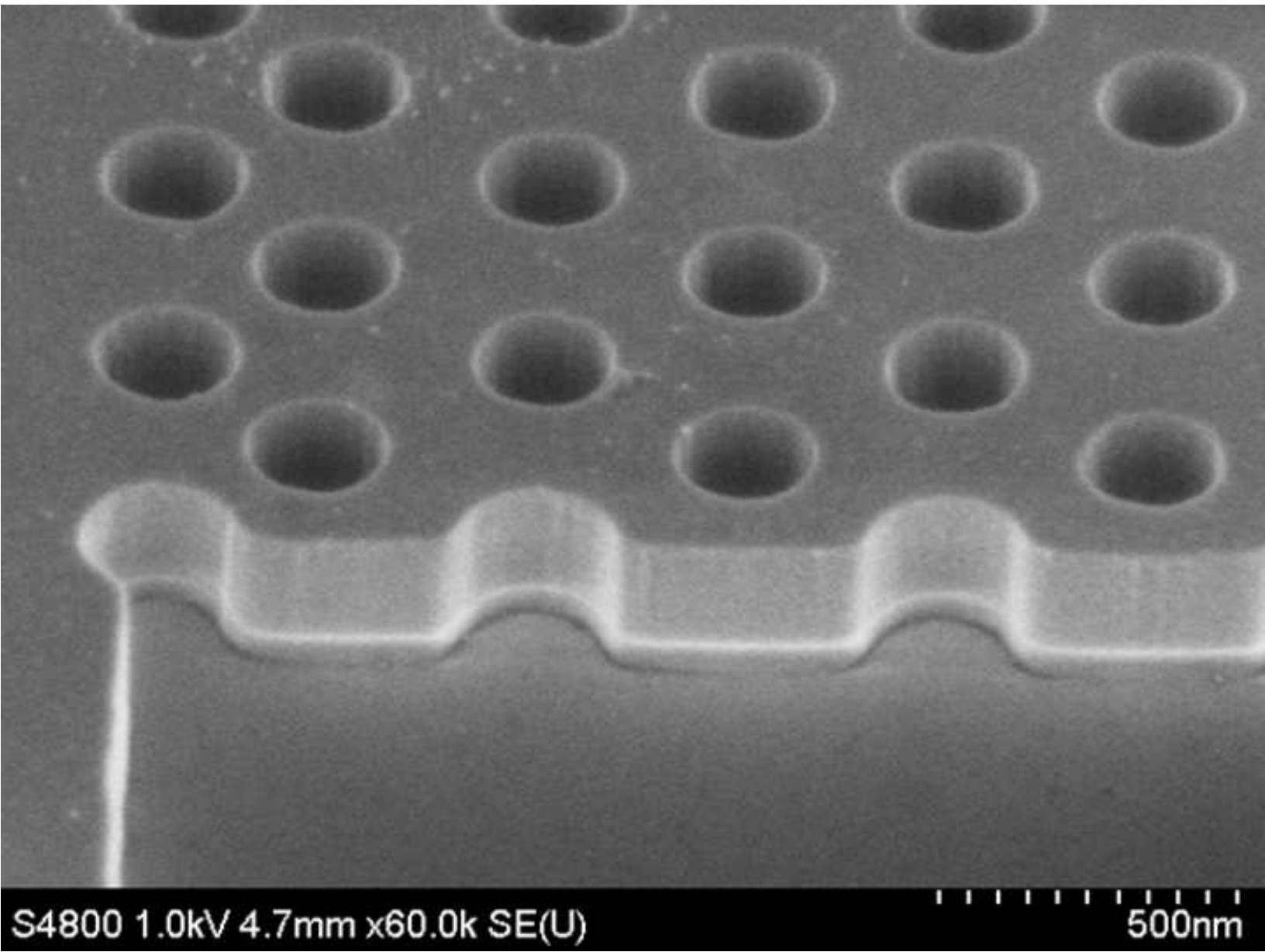

Figure 3: Photonic crystal waveguide after undercut etch with hy
Click here to download Figure: Fig03.eps

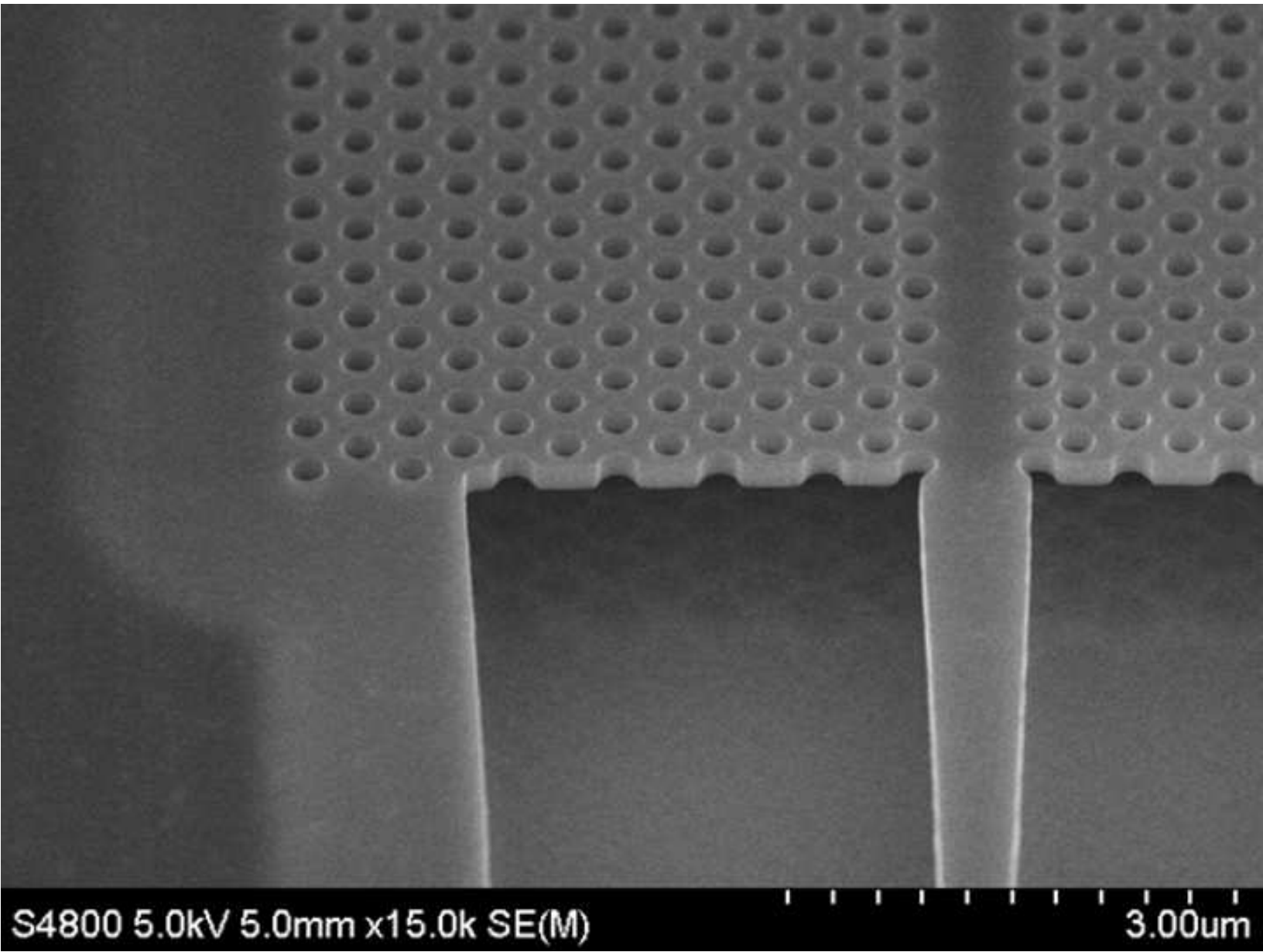

Figure 4: Photonic crystal in silicon etched with optimised RIE
Click here to download Figure: Fig04.eps

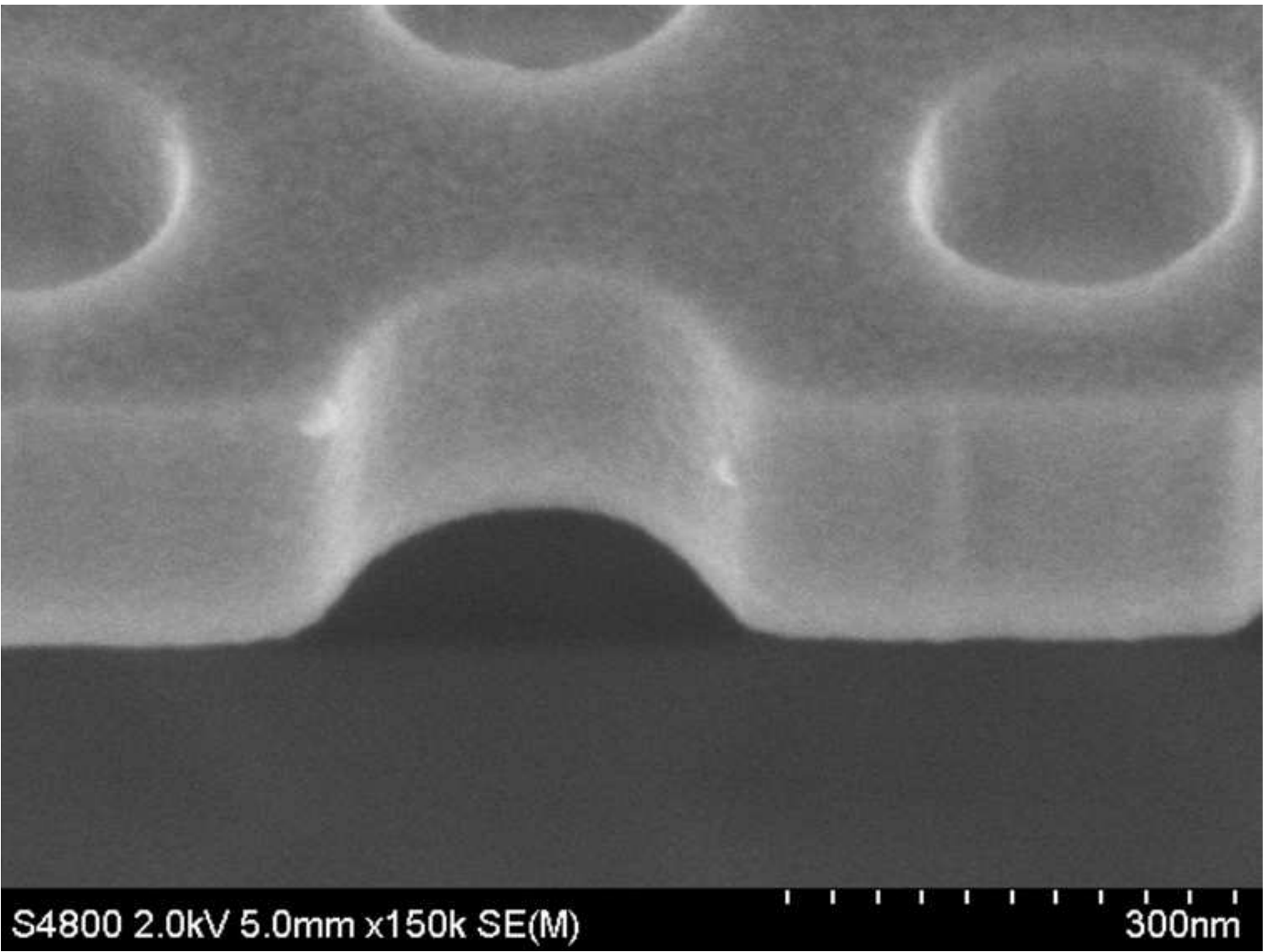

Figure 5: Photonic crystal etched with increased RIE chamber pre
Click here to download Figure: Fig05.eps

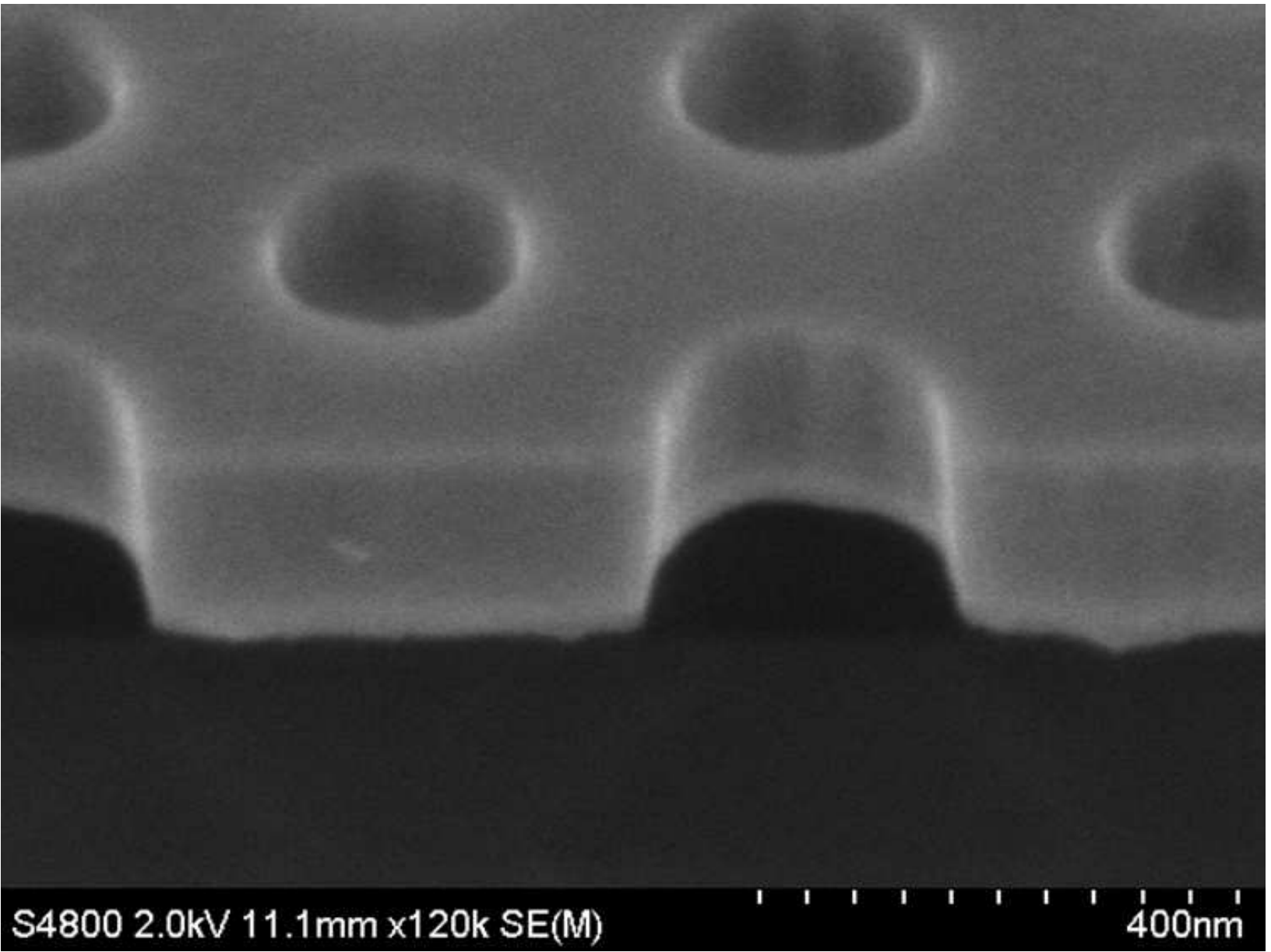

Figure 6: Photonic crystal etched with higher RF power (and DC b
Click here to download Figure: Fig06.eps

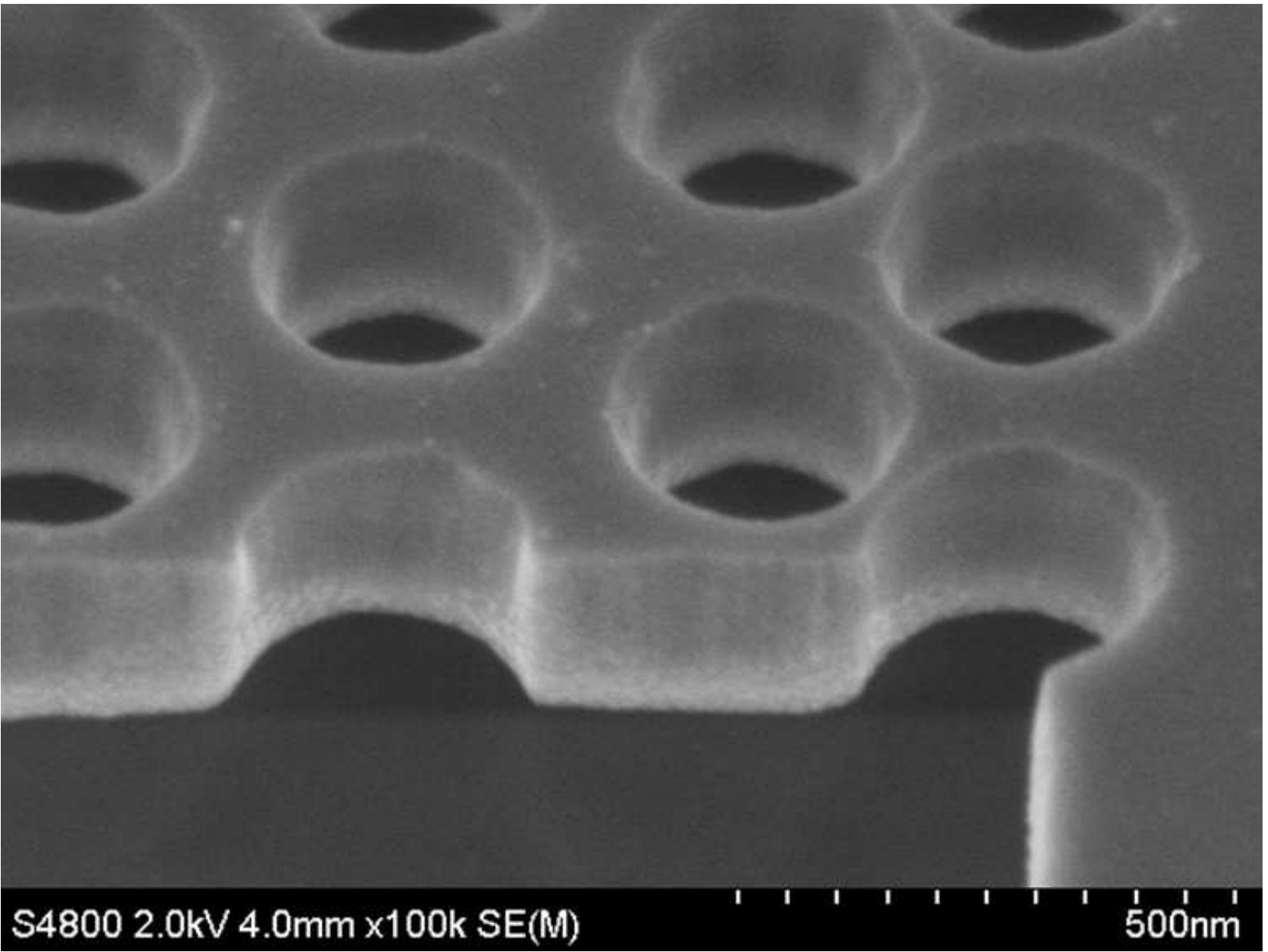

Figure 7: Over etched photonic crystal.  Angled side-walls due t
Click here to download Figure: Fig07.eps

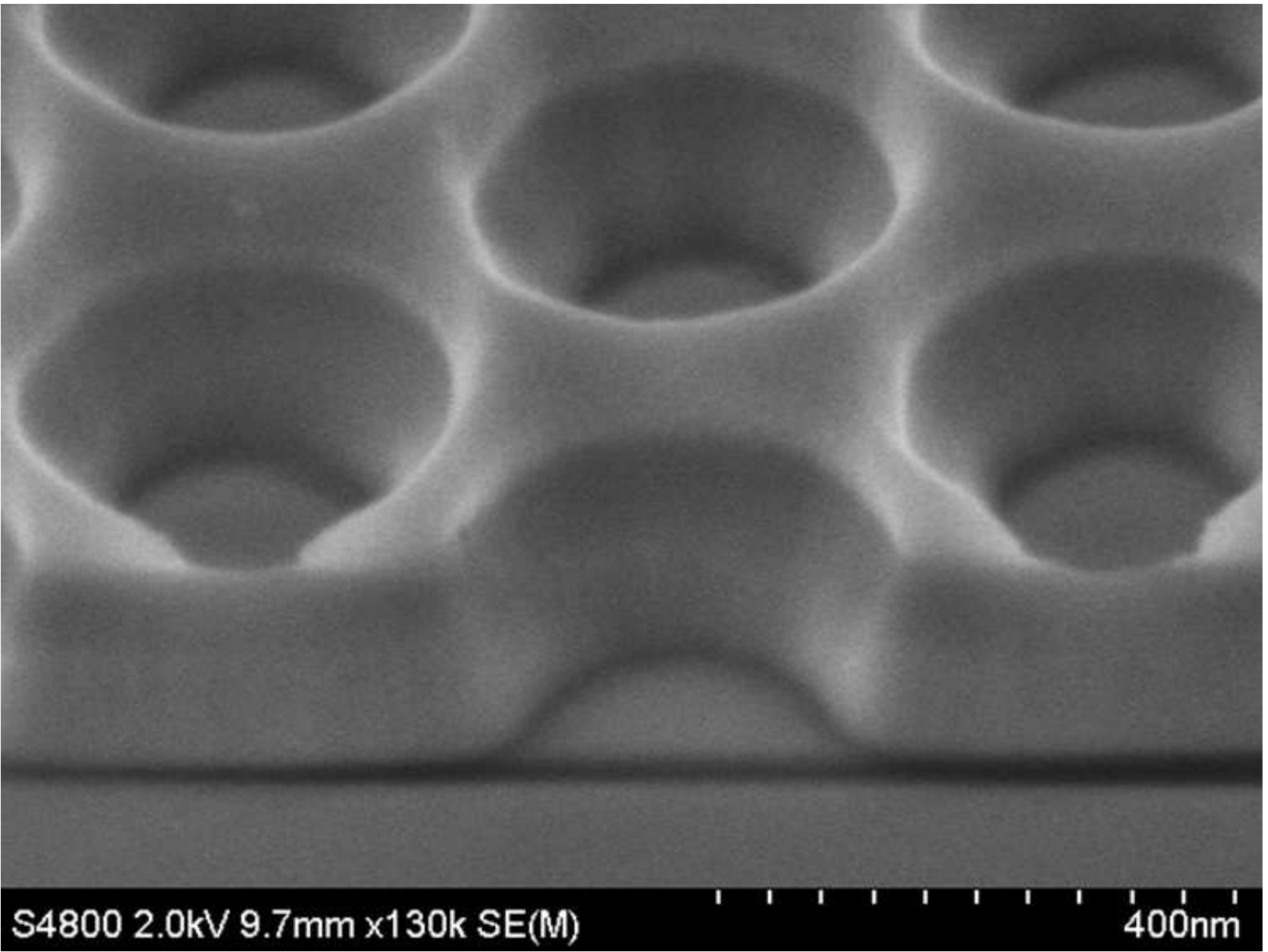

Figure 8: Poorly optimised etch (i.e. both pressure and time).
Click here to download Figure: Fig08.eps

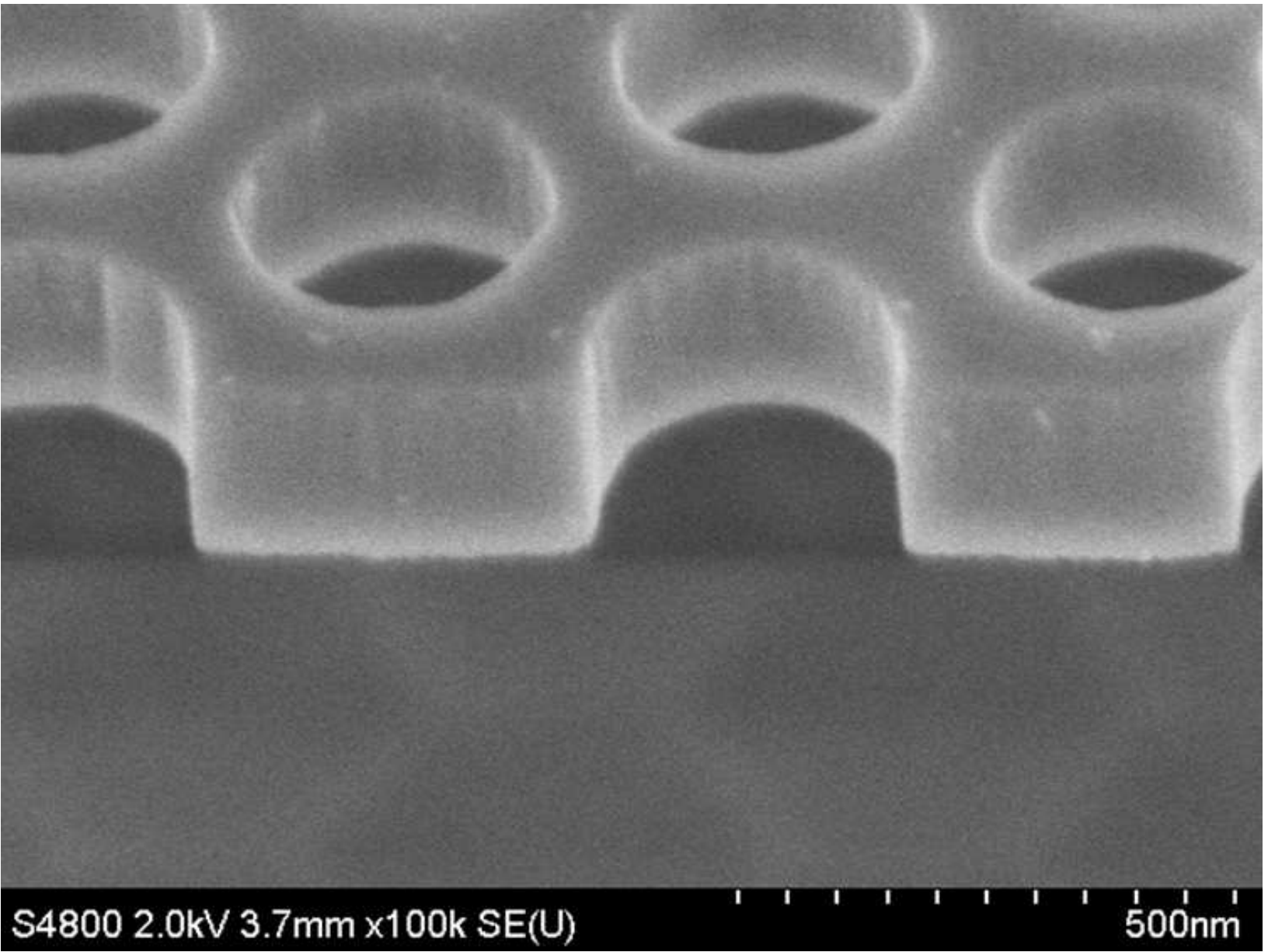

Figure 9: Schematic of the Mach-Zehnder interferometric setup us
Click here to download Figure: Fig09.eps

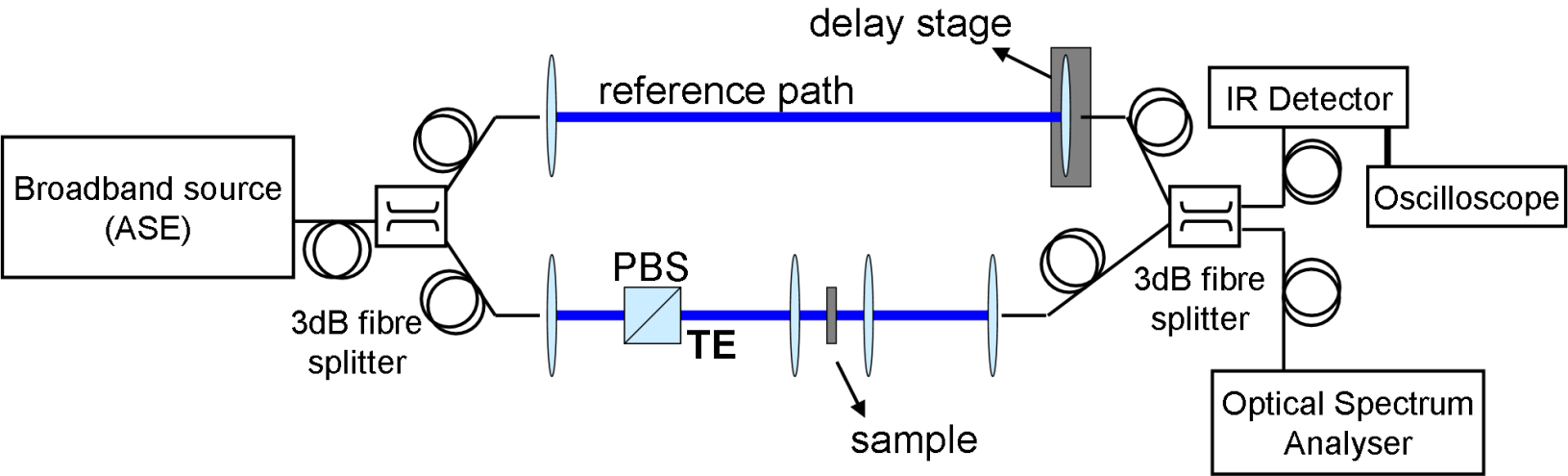

Figure 10: Measured interferograms of (a) a blank ridge waveguid
Click here to download Figure: Fig10.eps

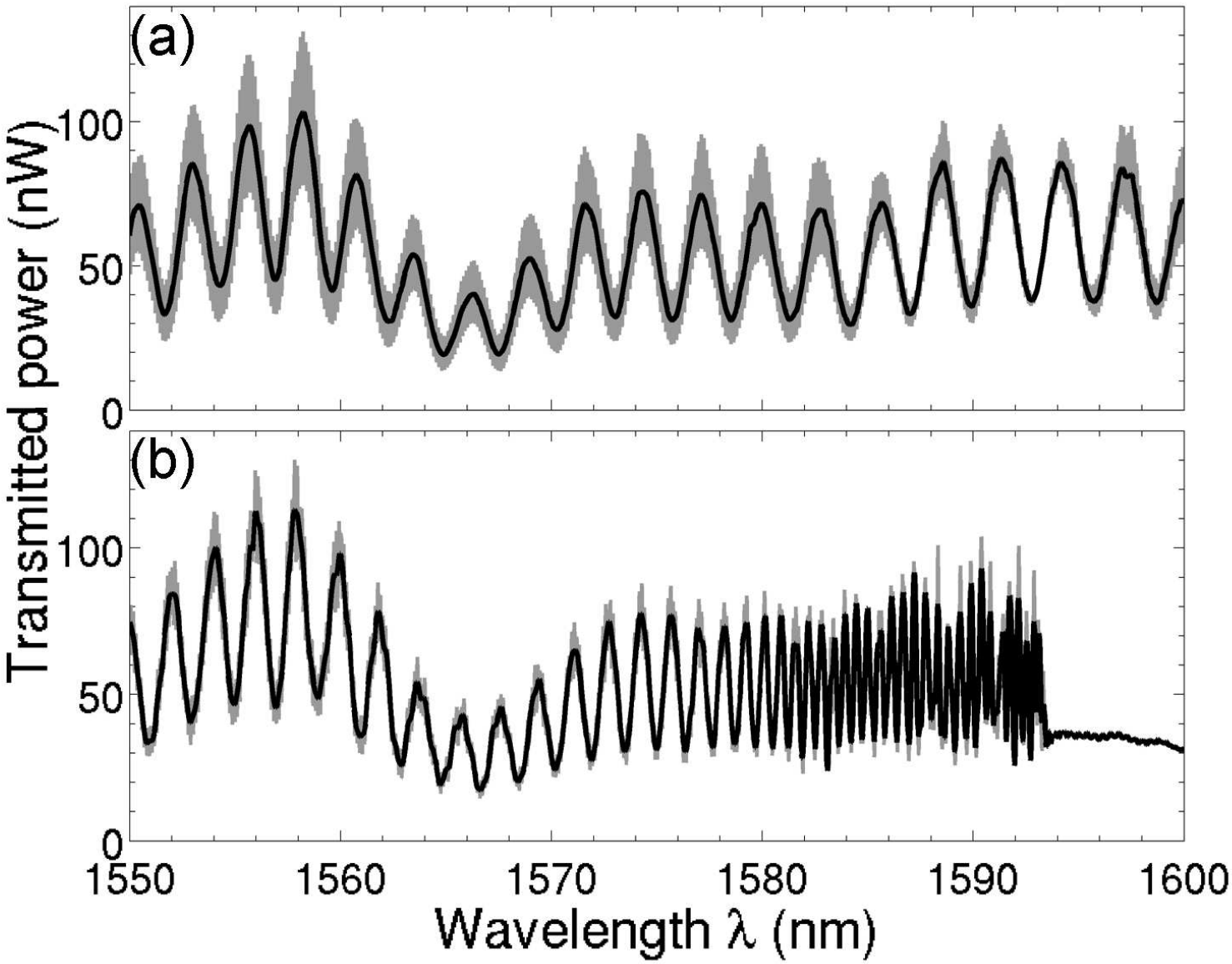

Figure 11: Group index (blue) and transmission (black, grey) cur
Click here to download Figure: Fig11.eps

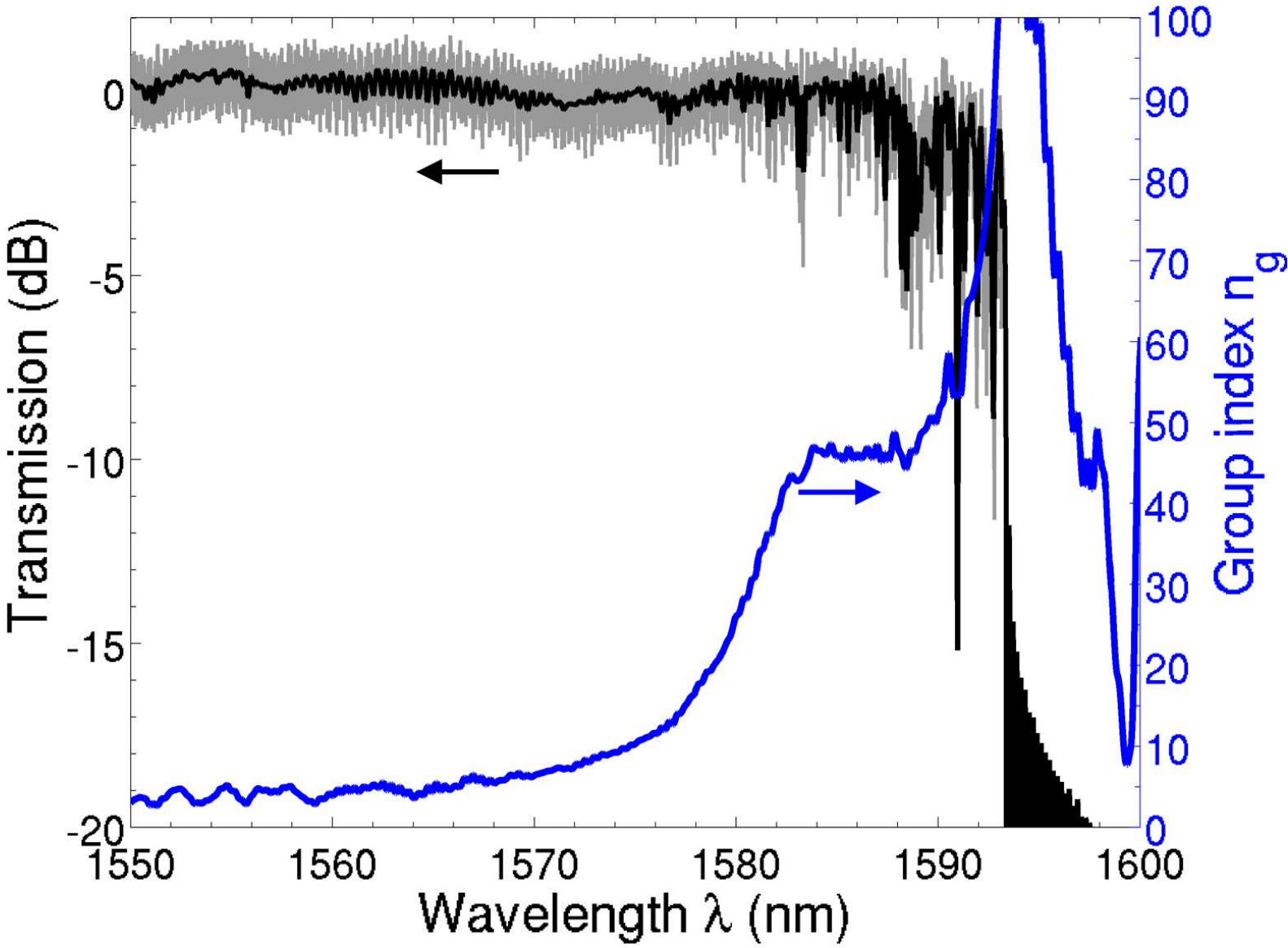

Figure 12: Group index (blue) and transmission (black, grey) cur
Click here to download Figure: Fig12.eps

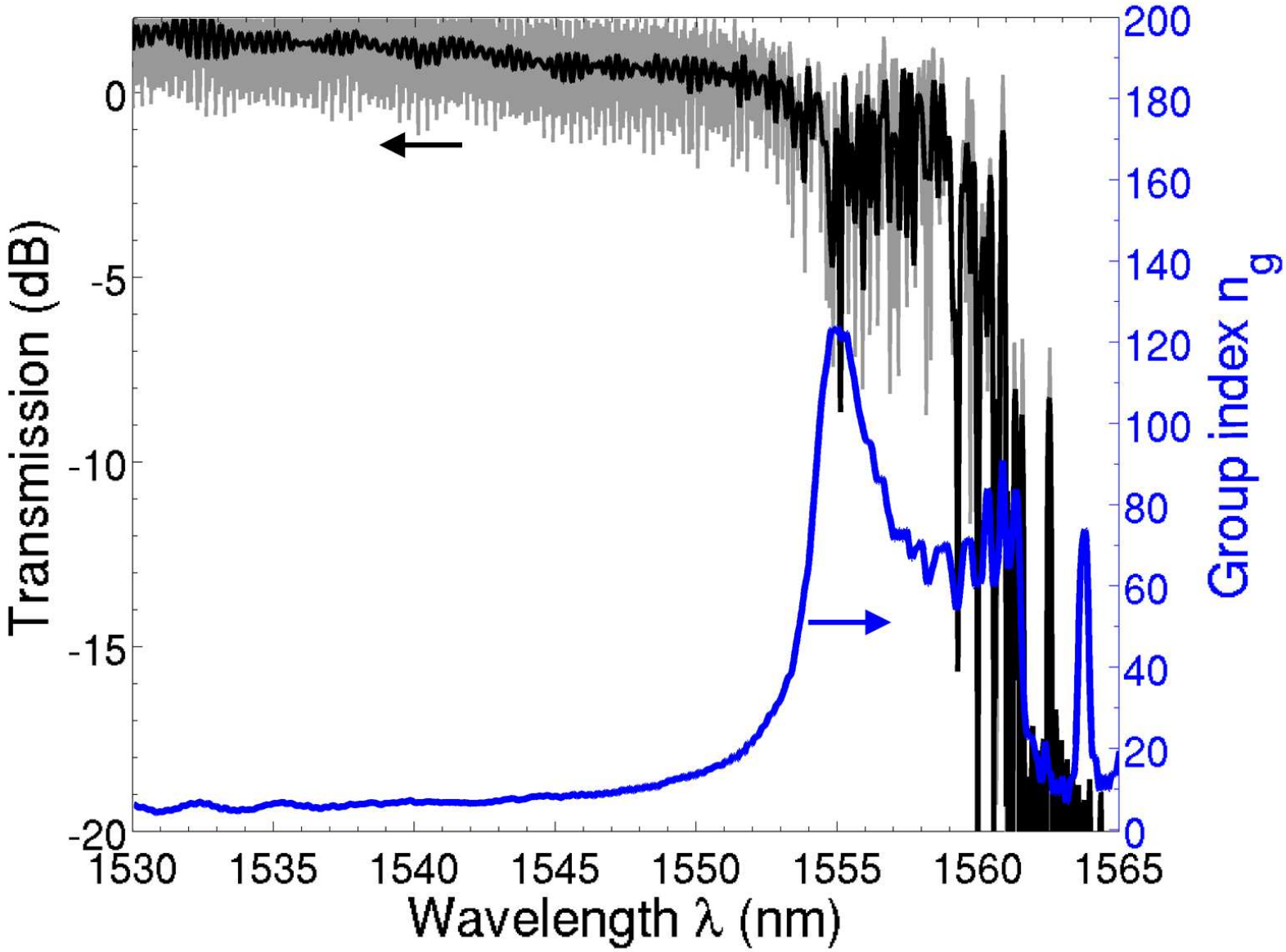

Figure 13: Group index (blue) and transmission (black, grey) cur
Click here to download Figure: Fig13.eps

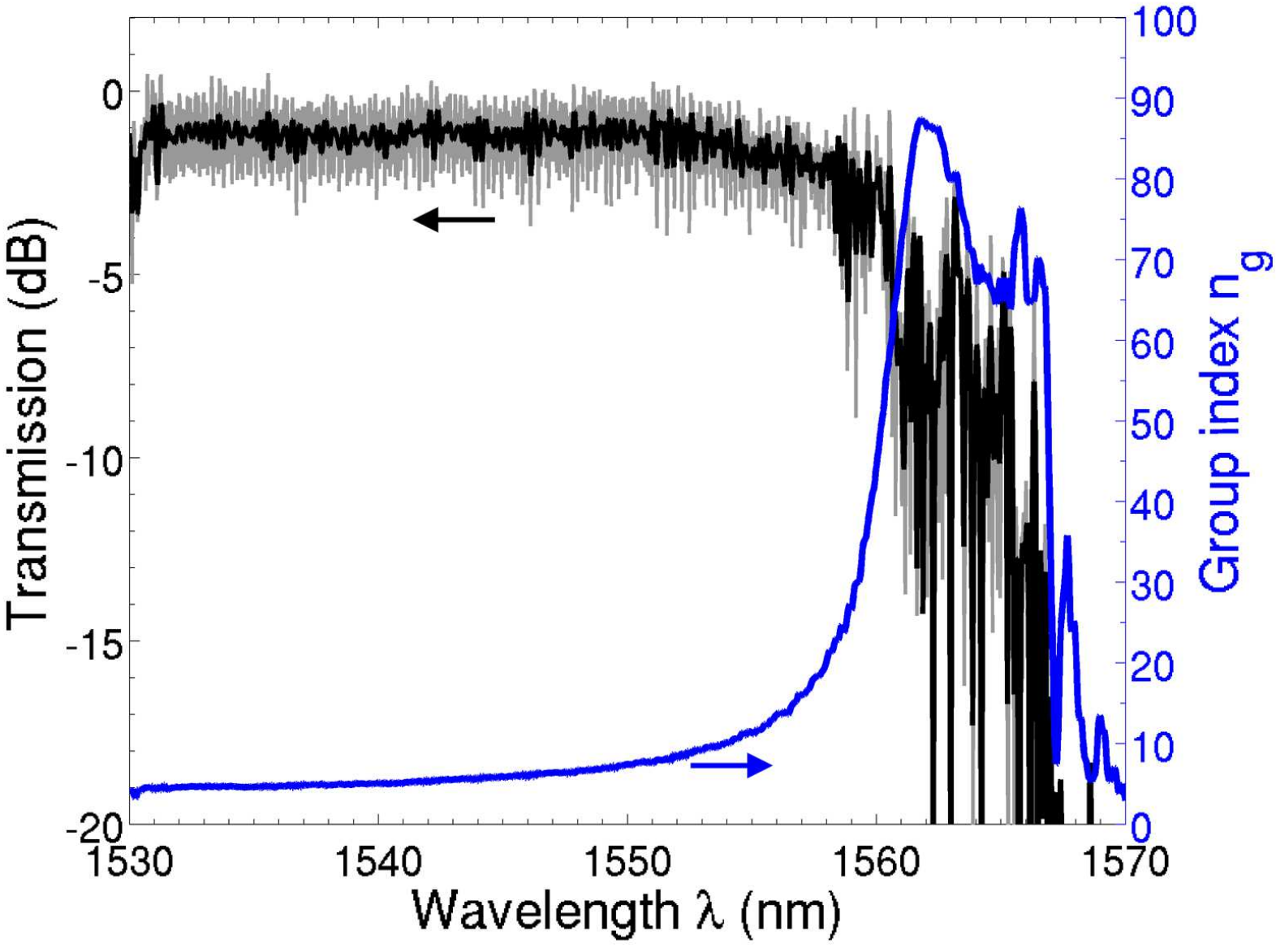

Figure 14: Top-view of multi-functional characterisation setup w
Click here to download high resolution image

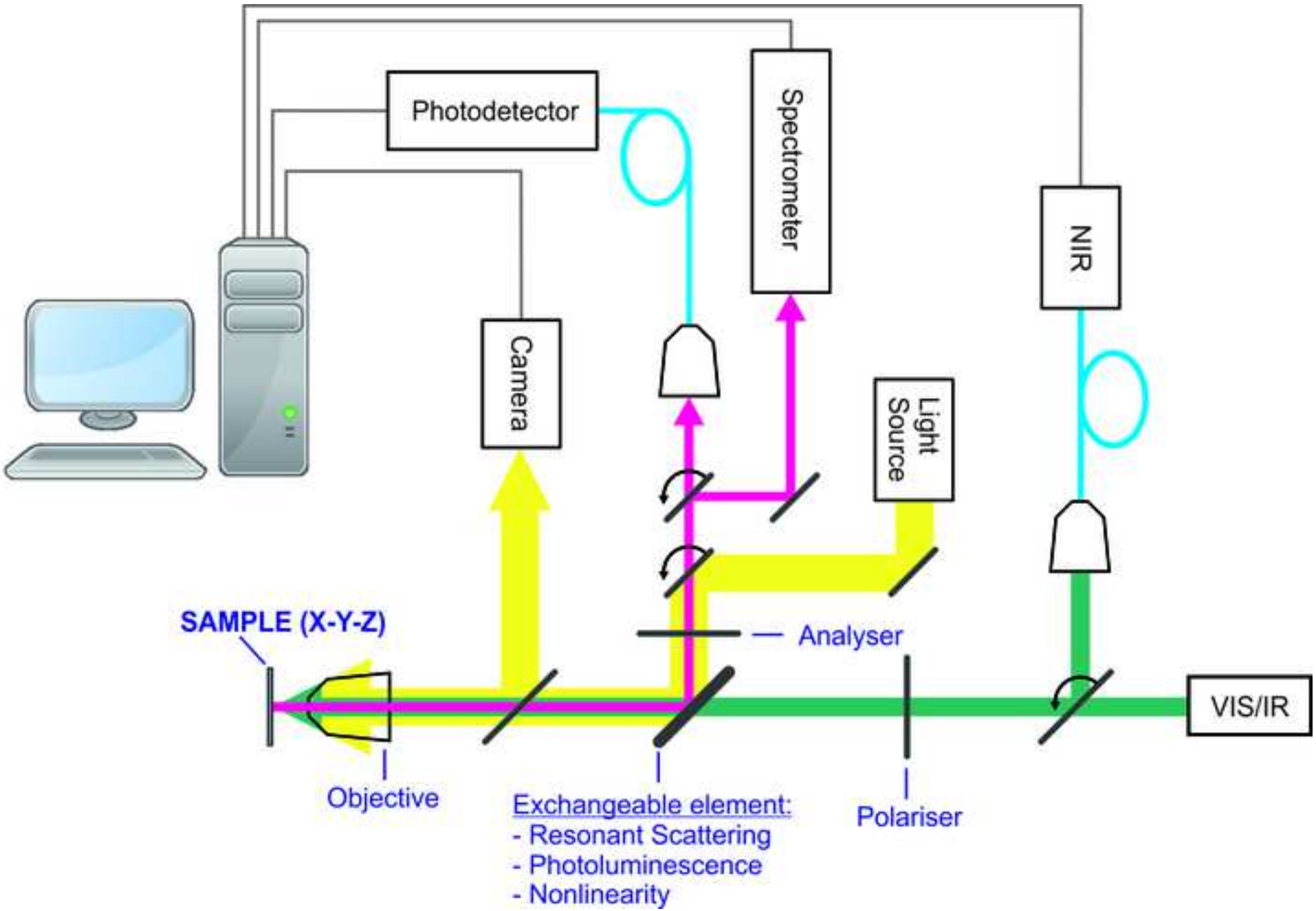

Figure 15: Captured image as appears on screen with beam off (le
Click here to download high resolution image

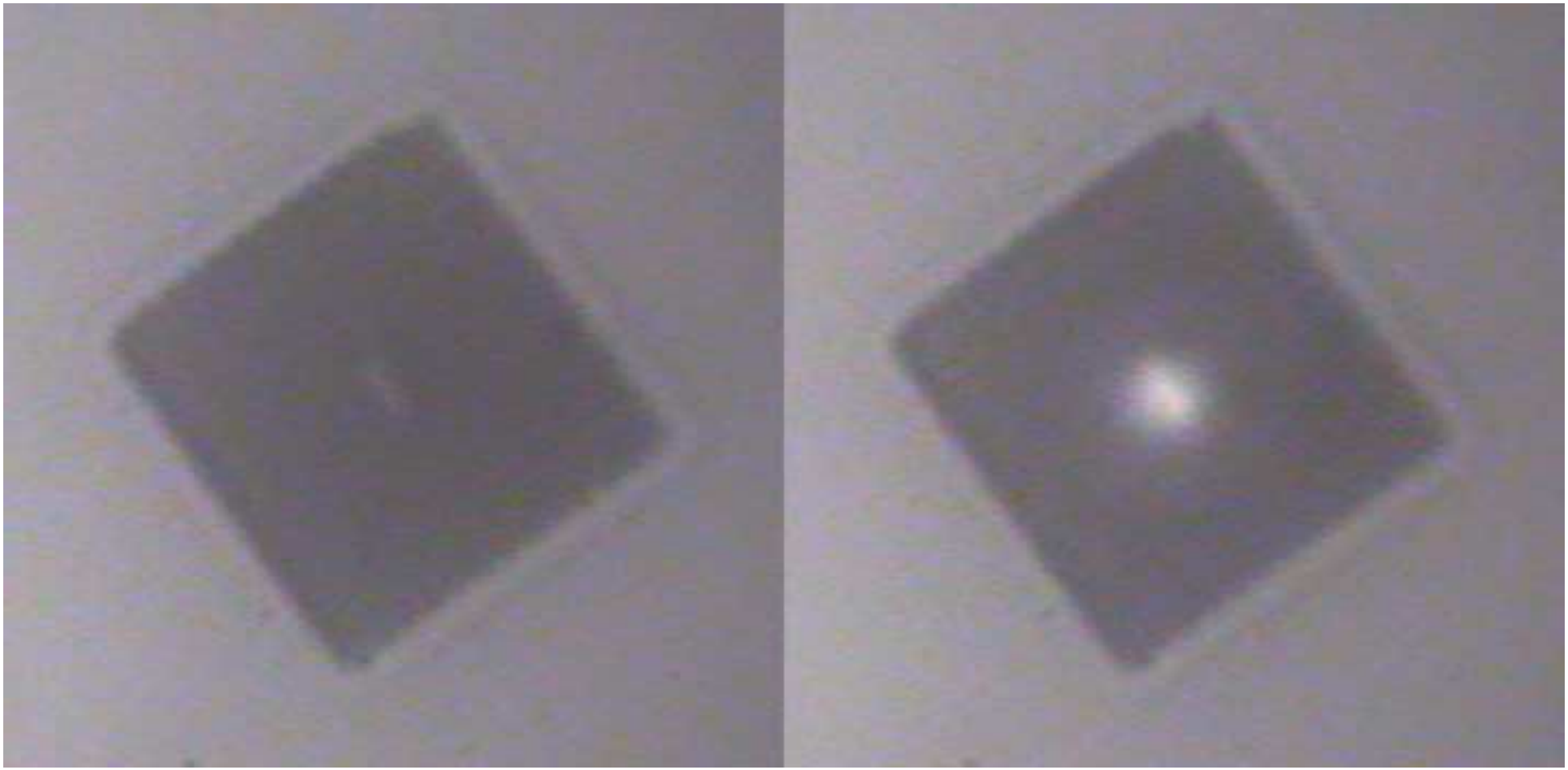

Figure 16: Initial broadband scan to identify the cavity resonan
Click here to download Figure: Fig16.eps

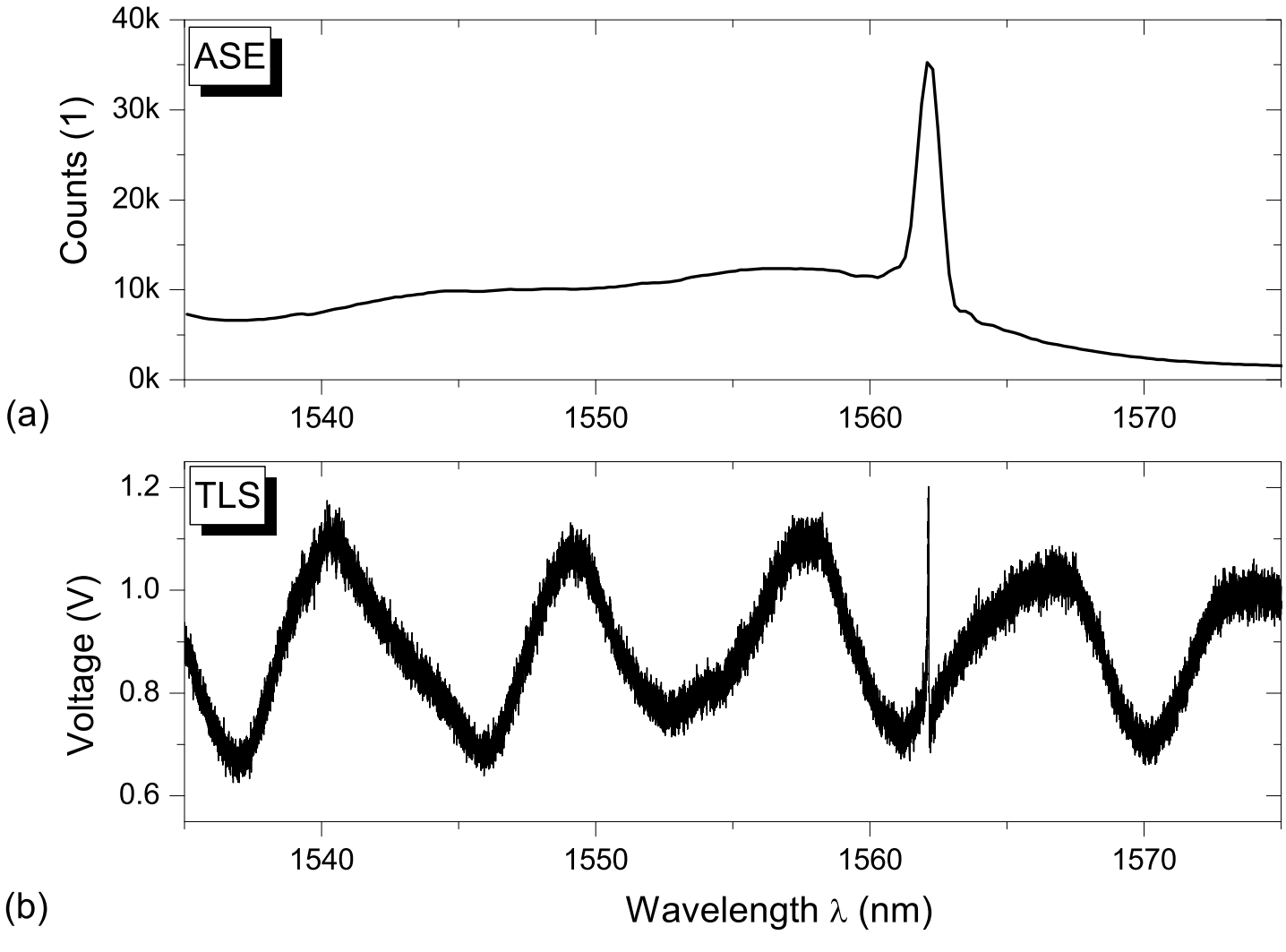

Figure 17: High-resolution scans with the TLS. (a) Lorentzian l
Click here to download Figure: Fig17.eps

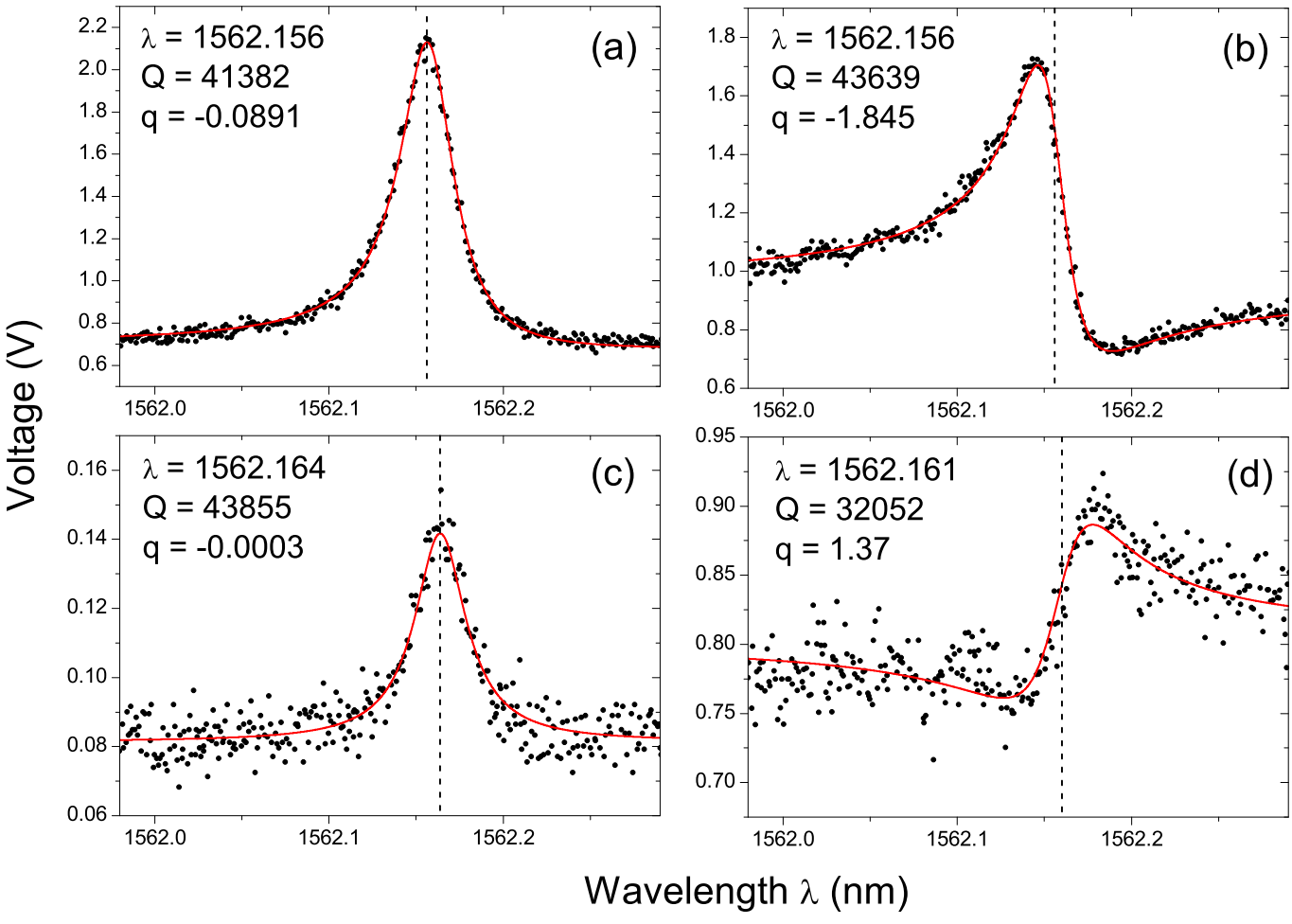

Figure 18: Arrangement of polarising optics (a) to the sample (b
Click here to download high resolution image

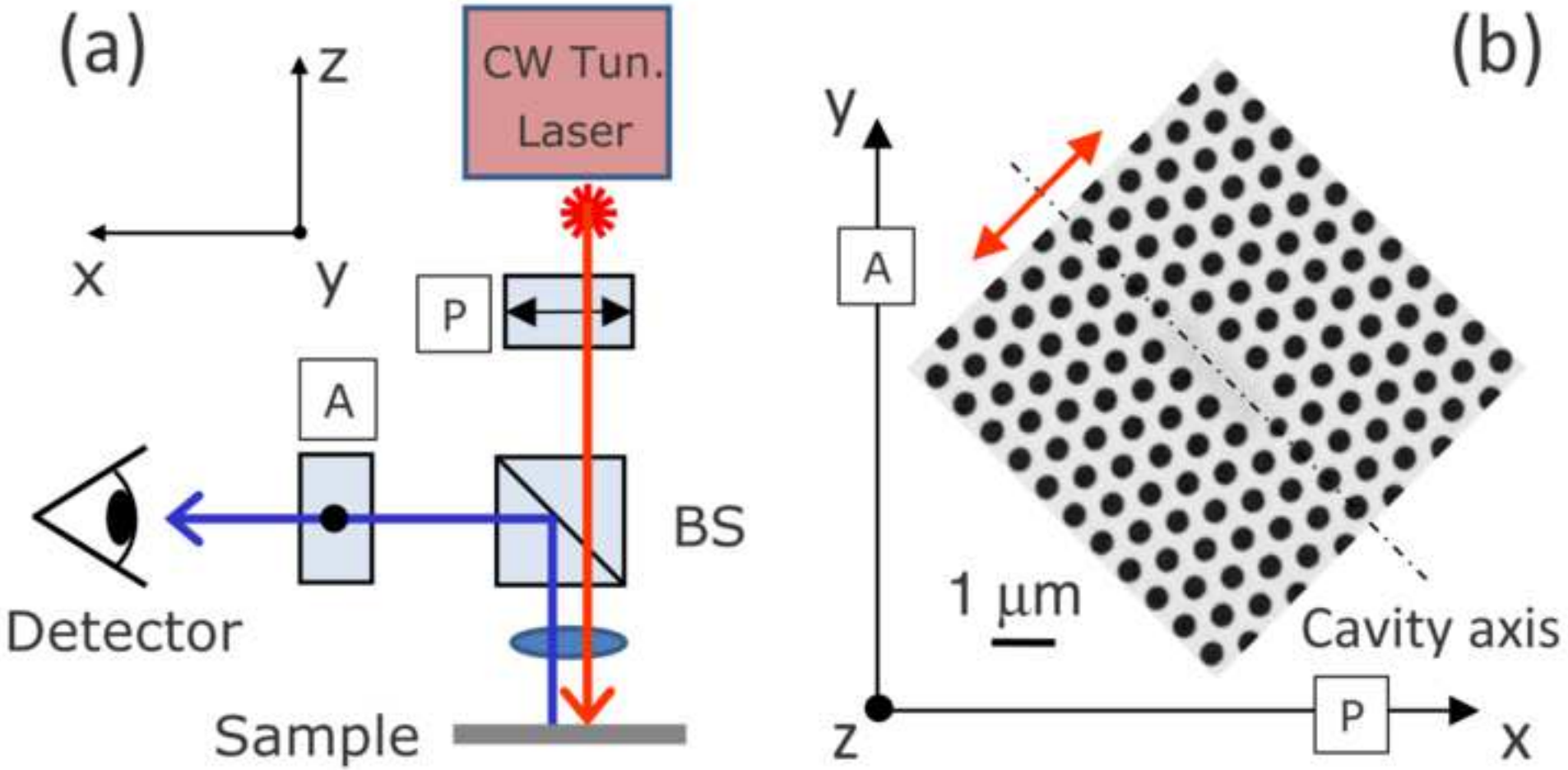

*Table of Reagents/ Materials Used

Click here to download Table of Reagents/ Materials Used: Materials_jove.xlsx

| Name of Reagent | Company | Catalog Number |
|---|---|---|
| Acetone | Fisher Scientific | A/0520/17 |
| Isopropanol | Fisher Scientific | P/7500/15 |
| Electron Beam resist | Marubeni Europe plc. | ZEP520A |
| Xylene | Fisher Scientific | X/0100/17 |
| Microposit S1818 G2 | Chestech Ltd. | 10277866 |
| Microposit Developer MF-319 | Chestech Ltd. | 10058721 |
| Hydrofluoric Acid | Fisher Scientific | 22333-5000 |
| Microposit 1165 Remover | Chestech Ltd. | 10058734 |
| Sulphuric Acid | Fisher Scientific | S/9120/PB17 |
| Hydrogen Peroxide | Fisher Scientific | BPE2633-500 |

| Name of Equipment | Company | Catalog Number |
|---|---|---|
| Silicon-on-Insulator wafer | Soitec | G8P-110-01 |
| Diamond Scribe | J & M Diamond Tool Inc. | HS-415 |
| Microscope slides | Fisher Scientific | FB58622 |
| Beakers | Fisher Scientific | FB33109 |
| Tweezers | SPI Supplies | PT006-AB |
| Ultrasonic Bath | Camlab | 1161436 |
| Spin-Coater | Electronic Micro Systems Ltd. | EMS 4000 |
| Pipette | Fisher Scientific | FB55343 |
| E-beam Lithography System | Raith Gmbh | Raith 150 |
| Reactive Ion Etching System | Proprietary In-house Designed | -- |
| UV Mask Aligner | Karl Suss | MJB-3 |
| ASE source | Amonics | ALS-CL-15-B-FA |
| Single mode fibres | Thorlabs | P1-SMF28E-FC-2 |
| 3dB fibre splitters | Thorlabs | C-WD-AL-50-H-2210-35-FC/FC |
| Aspheric lenses | New Focus | 5720-C |
| XYZ stages | Melles Griot | 17AMB003/MD |
| Polarising beamsplitter cube | Thorlabs | PBS104 |
| IR detector | New Focus | 2033 |
| 100× Objective | Nikon | BD Plan 100x |

| | | |
|---|---|---|
| Oscilloscope | Tektronix | TDS1001B |
| Optical Spectrum Analyser | Advantest | Q8384 |
| IR sensor card | Newport | F-IRC2 |
| ASE source | Alpha Photonics | ALS-CL-15-B-FA |
| TLS source | Agilent | 81940A |
| IR Camera | Electrophysics | 7290A |
| IR Detector | New Focus | 2153 |
| Digital Multimeter | Agilent | 34401A |
| Illumination | Stocker Yale | Lite Mite |
| Monochromator | Spectral Products | DK480 |
| Array Detector | Andor | DU490A-1.7 |
| GIF Fibre | Thorlabs | 31L02 |

**Comments**

| |
|---|
| CAUTION: flammable, use good ventilation and avoid all ignition sources |
| CAUTION: flammable, use good ventilation and avoid all ignition sources |
| CAUTION: flammable, harmful by inhalation, avoid contact with skin and eyes |
| CAUTION: flammable and highly toxic, use good ventilation, avoid all ignition sources, avoid contact with skin and eyes |
| CAUTION: flammable and causes irritation to eyes, nose and respiratory tract |
| CAUTION: alkaline liquid and can cause irritation to eyes, nose and respiratory tract |
| CAUTION: extremely corrosive, readily destroys tissue; handle with full personal protective equipment rated for HF |
| CAUTION: flammable and causes irritation to eyes, nose and respiratory tract |
| CAUTION: corrosive and very toxic; handle with personal protective equipment and avoid inhalation of vapours or mists |
| CAUTION: very hazardous in case of skin and eye contact; handle with personal protective equipment |

**Comments**

| |
|---|
| |
| |
| |
| |
| |
| |
| |
| |
| |
| |

| |
|---|
| CAUTION: invisible IR radiation |
| |
| |
| |
| |
| |
| |
| |

CAUTION: invisible IR radiation

17 Sellers Street
Cambridge, MA 02139
tel. +1.617.945.9051
www.JoVE.com

# ARTICLE AND VIDEO LICENSE AGREEMENT

Title of Article: FABRICATION AND CHARACTERISATION OF BOTH PHOTONIC CRYSTAL SLOW LIGHT WAVEGUIDES AND CAVITIES

Author(s): CHRISTOPHER P REARDON, ISABELLA H REY, KARL WELNA, LIAM O'FAOLAIN, THOMAS F. KRAUSS

Item 1 (check one box): The Author elects to have the Materials be made available (as described at http://www.jove.com/publish ) via: [X] Standard Access [ ] Open Access

Item 2 (check one box):

[X] The Author is NOT a United States government employee.

[ ] The Author is a United States government employee and the Materials were prepared in the course of his or her duties as a United States government employee.

[ ] The Author is a United States government employee but the Materials were NOT prepared in the course of his or her duties as a United States government employee.

## ARTICLE AND VIDEO LICENSE AGREEMENT

1. Defined Terms. As used in this Article and Video License Agreement, the following terms shall have the following meanings: "**Agreement**" means this Article and Video License Agreement; "**Article**" means the article specified on the last page of this Agreement, including any associated materials such as texts, figures, tables, artwork, abstracts, or summaries contained therein; "**Author**" means the author who is a signatory to this Agreement; "**Collective Work**" means a work, such as a periodical issue, anthology or encyclopedia, in which the Materials in their entirety in unmodified form, along with a number of other contributions, constituting separate and independent works in themselves, are assembled into a collective whole; "**CRC License**" means the Creative Commons Attribution-Non Commercial-No Derivs 3.0 Unported Agreement, the terms and conditions of which can be found at: http://creativecommons.org/licenses/by-nc-nd/3.0/legalcode; "**Derivative Work**" means a work based upon the Materials or upon the Materials and other pre-existing works, such as a translation, musical arrangement, dramatization, fictionalization, motion picture version, sound recording, art reproduction, abridgment, condensation, or any other form in which the Materials may be recast, transformed, or adapted; "**Institution**" means the institution, listed on the last page of this Agreement, by which the Author was employed at the time of the creation of the Materials; "**JoVE**" means MyJove Corporation, a Massachusetts corporation and the publisher of *The Journal of Visualized Experiments;* "**Materials**" means the Article and / or the Video; "**Parties**" means the Author and JoVE; "**Video**" means any video(s) made by the Author, alone or in conjunction with any other parties, or by JoVE or its affiliates or agents, individually or in collaboration with the Author or any other parties, incorporating all or any portion of the Article, and in which the Author may or may not appear.

2. Background. The Author, who is the author of the Article, in order to ensure the dissemination and protection of the Article, desires to have the JoVE publish the Article and create and transmit videos based on the Article. In furtherance of such goals, the Parties desire to memorialize in this Agreement the respective rights of each Party in and to the Article and the Video.

3. Grant of Rights in Article. In consideration of JoVE agreeing to publish the Article, the Author hereby grants to JoVE, subject to **Sections 4** and **7** below, the exclusive, royalty-free, perpetual (for the full term of copyright in the Article, including any extensions thereto) license (a) to publish, reproduce, distribute, display and store the Article in all forms, formats and media whether now known or hereafter developed (including without limitation in print, digital and electronic form) throughout the world, (b) to translate the Article into other languages, create adaptations, summaries or extracts of the Article or other Derivative Works (including, without limitation, the Video) or Collective Works based on all or any portion of the Article and exercise all of the rights set forth in (a) above in such translations, adaptations, summaries, extracts, Derivative Works or Collective Works and (c) to license others to do any or all of the above. The foregoing rights may be exercised in all media and formats, whether now known or hereafter devised, and include the right to make such modifications as are technically necessary to exercise the rights in other media and formats. If the "Open Access" box has been checked in **Item 1** above, JoVE and the Author hereby grant to the public all such rights in the Article as provided in, but subject to all limitations and requirements set forth in, the CRC License.

4. Retention of Rights in Article. Notwithstanding the exclusive license granted to JoVE in **Section 3** above, the

jove JOURNAL OF VISUALIZED EXPERIMENTS
17 Sellers Street
Cambridge, MA 02139
tel. +1.617.945.9051
www.JoVE.com

# ARTICLE AND VIDEO LICENSE AGREEMENT

without limitation, to all decisions regarding editing, lighting, filming, timing of publication, if any, length, quality, content and the like.

11. Indemnification. The Author agrees to indemnify JoVE and/or its successors and assigns from and against any and all claims, costs, and expenses, including attorney's fees, arising out of any breach of any warranty or other representations contained herein. The Author further agrees to indemnify and hold harmless JoVE from and against any and all claims, costs, and expenses, including attorney's fees, resulting from the breach by the Author of any representation or warranty contained herein or from allegations or instances of violation of intellectual property rights, damage to the Author's or the Author's institution's facilities, fraud, libel, defamation, research, equipment, experiments, property damage, personal injury, violations of institutional, laboratory, hospital, ethical, human and animal treatment, privacy or other rules, regulations, laws, procedures or guidelines, liabilities and other losses or damages related in any way to the submission of work to JoVE, making of videos by JoVE, or publication in *JoVE* or elsewhere by JoVE. The Author shall be responsible for, and shall hold JoVE harmless from, damages caused by lack of sterilization, lack of cleanliness or by contamination due to the making of a video by JoVE its employees, agents or independent contractors. All sterilization, cleanliness or decontamination procedures shall be solely the responsibility of the Author and shall be undertaken at the Author's expense. All indemnifications provided herein shall include JoVE's attorney's fees and costs related to said losses or damages. Such indemnification and holding harmless shall include such losses or damages incurred by, or in connection with, acts or omissions of JoVE, its employees, agents or independent contractors.

12. Fees. To cover the cost incurred for publication, JoVE must receive payment before production and publication the Materials. Payment is due in 21 days of invoice. Should the Materials not be published due to an editorial or production decision, these funds will be returned to the Author. Withdrawal by the Author of any submitted Materials after final peer review approval will result in a US$1,200 fee to cover pre-production expenses incurred by JoVE. If payment is not received by the completion of filming, production and publication of the Materials will be suspended until payment is received.

13. Transfer, Governing Law. This Agreement may be assigned by JoVE and shall inure to the benefits of any of JoVE's successors and assignees. This Agreement shall be governed and construed by the internal laws of the Commonwealth of Massachusetts without giving effect to any conflict of law provision thereunder. This Agreement may be executed in counterparts, each of which shall be deemed an original, but all of which together shall be deemed to me one and the same agreement. A signed copy of this Agreement delivered by facsimile, e-mail or other means of electronic transmission shall be deemed to have the same legal effect as delivery of an original signed copy of this Agreement.

A signed copy of this document must be sent with all new submissions. Only one Agreement required per submission.

**AUTHOR:**

Name: CHRISTOPHER REARDON

Department: SCHOOL OF PHYSICS & ASTRONOMY

Institution: UNIVERSITY OF ST ANDREWS

Article Title: FABRICATION AND CHARACTERISATION OF BOTH PHOTONIC CRYSTAL SLOW LIGHT WAVEGUIDES AND CAVITIES

Signature: CReardon Date: 6-7-2012

Please submit a signed and dated copy of this license by one of the following three methods:

1) Upload a scanned copy as a PDF to the *JoVE* submission site upon manuscript submission (preferred);
2) Fax the document to +1.866.381.2236; or
3) Mail the document to *JoVE* / Attn: *JoVE* Editorial / 17 Sellers St / Cambridge, MA 02139

For questions, please email editorial@jove.com or call +1.617.945.9051.

MS # (internal use):

Dear Editor,

**RE: JoVE50216 'Fabrication and Characterisation of both Photonic Crystal Slow Light Waveguides and Cavities'**

First we would like to thank you for the opportunity to publish our work within the journal of visualized experiments. We would also like to thank the referees for taking the time to read our submission, we agree with the referees' comments and where we feel appropriate have amended our paper to make their and our points clearer. Our answers to the referees and our corrections can be seen below and within the re-submitted manuscript.

Yours sincerely,

Christopher Reardon, Isabella Rey, Karl Welna, Liam O'Faolain and Thomas Krauss

**Reviewer #1:**

*Minor Concerns:*

We thank the reviewer for their comments and agree with their suggestion of dropping "both" from our paper's title. The title now reads: "Fabrication and Characterisation of Photonic Crystal Slow Light Waveguides and Cavities".

We appreciate the reviewers remark as to our fabrication techniques being applicable not only to silicon but to other semiconductors, as such we have included the following: "*Although the protocol outlined in this paper is optimised for SOI, the general principle behind the fabrication methods are also valid for the fabrication of devices into other semiconductors: of course, when changing from silicon, careful consideration of etch-tool, etch-chemistries and mask materials would need to be made.*" within the "Sample fabrication" discussion section of the paper.

We thank the referee for his suggestion to add more background information on slow light and resonant cavities. A new paragraph now appears at the beginning of the discussion section on slow light, where we have also added a new Reference [34]: *"The significance of the group index as the key parameter to measure slow light originates from the dispersion diagram or band structure ω(k) typically used to describe the dispersion of a photonic crystal waveguide.*[34] *The local slope of the dispersion curve ∂ω/∂k corresponds to the group velocity* $v_g$*, i.e. the speed at which the electromagnetic energy travels through the waveguide, which can be equivalently described by the group index* $n_g=c/v_g$*. Values of* $n_g$ *around 5 correspond to the fast light regime, whereas higher values are typically considered to fall within in the slow light regime."* As for resonant cavities we have added the following: *"Photonic crystal cavities confine light in-plane in two dimensions, in contrast to photonic crystal waveguides, where light is guided in one dimension. This allows the storage*

*of light within ultra-small volumes, which is described by an energy decay, analogue to i.e. that of an electronic resonator. In photonic systems, this decay is associated with the photon lifetime of the cavity and is of exponential form, hence resulting in a Lorentzian lineshape of the peak. The ratio of the peak centre wavelength to the Full-Width Half-Maximum represents the Q-factor."* However, we do not feel that introducing illustrations of the mode profiles would aid our audience to better understand the measurement techniques described here, which focus on characterisation of wavelength spectra.

**Reviewer #2:**

*Minor Concerns:*

We thank the reviewer for his kind remarks and agree that 'set-up the exposure as per the system's user-manual' could be confusing. We felt that including a detailed protocol focussed on the set-up of our EBL system (i.e. loading, measuring the sample, focussing the electron-beam, setting dose requirements and calculating dwell times, etc.) would be counter-productive as potentially the reader's system could be very different. However, hopefully the following sentence, now included in the paper, makes our point clearer: *"Set-up the exposure as indicated in the user-manual of your specific electron beam lithography system."*

We agree with the reviewer that our cleaning protocol may well be specific to our exact system. As such, we have now included the following details as to our RIE system: *"This procedure is optimised for our system which consists of a parallel-plate, cathode loaded RIE, with a main chamber 12 inches in diameter by 14 inches in height, including a 12 inch port with both throttling valve and turbo-molecular pump attached."*

The resulting etch rate of silicon using our specific RIE and parameters is 150 nm/min – we have now included the following statement into the paper to highlight this fact: *"…*etch the sample for approximately 2min (the etch rate of silicon for these etch parameters is approximately 150nm/min), while ensuring that a…*"* The etch rate between waveguide trenches and photonic crystal holes is different. Trenches etch faster than holes mainly due to the relative ease at which volatile silicon species, from the trench, can be removed by the pumping system of the RIE. Our protocol is optimised for the most critical part of our device, namely the photonic crystal. If the etching of waveguides alone was required, a new protocol (based upon the one outlined in this paper) may require optimisation.

We agree with the reviewer about our protocol sub-section 3.3 which does not make it clear that this procedure's purpose is the removal of any remaining ZEP. To avoid further confusion we have altered the sub-section to now read: *"Sample Cleaning to remove remaining electron sensitive resist – after dry…"*

In answer to the reviewer's point about our discussion section. The mis-alignment due to thermal instabilities within the e-beam lithography system can be as high as 100 nm/min in absolute terms. While this is quite a substantial error which would result in large losses within any photonic crystal device, a number of other points must be taken into account: namely, the beam drift is not entirely random, in that the position error of one hole is related to the position of the following and preceding hole. For example, if one hole is out of position by 5 nm the next hole will be out of position by either 4 or 6nm (assuming a 1 nm per hole drift), thus considerably reducing the hole-to-hole error and consequently the attributed loss. Secondly, the speed at which the machine writes each hole also has an effect, as it is the ratio between the rate at which holes are exposed and the beam drift that determines the hole misplacement, i.e. for the same beam drift (thermal instability), a faster beam speed reduces the positioning errors. To make this point clearer, within the sample fabrication discussion we have added/amended the following: *"…chamber (even at only a few nanometres per photonic crystal hole) results in significant stitching and possibly pattern distortion errors with respect to photonic crystal tolerances. This error is random in nature, from one exposure to another, but can be as high as 100 nm/min (absolute positional error). The relative positional error (i.e. between one photonic crystal hole to another) can be on the order of nanometres, which can be further reduced by increasing the speed at which the pattern is written. These issues can be further negated (although never completely removed) by allowing the system to settle after first loading the sample."*

The use of $Ar/H_2$ plasma and $O_2$ plasma is due to their different etching properties. $Ar/H_2$ are used due to their ion-bombardment capabilites and are able through ion milling to clean the RIE chamber of most general contaminants (i.e. metal residue, silicon residue, etc.). $O_2$ plasma is used instead in an ashing capacity, to remove any remaining polymers or organics from the chamber. To highlight these two points the sample fabrication discussion has been amended to read: *"…$Ar/H_2$ plasma etch (used to remove metal and silicon contaminants through ion bombardment) followed by $O_2$ plasma etch (used for the removal of polymer and organic residue through plasma ashing) described…"*

**Reviewer #3:**

*Major Concerns:*

We thank the reviewer for their remarks and would like to answer them. The functional wavelength range of our proposed photonic crystals is centred at 1550nm as we, as a research group, have focussed on the wavelengths of interest to the telecoms industry. We now regularly fabricate photonic crystals that target the 2.7–3.5μm range which, however, require different substrates i.e. an SOI wafer with both a thicker silicon top-layer and buried oxide layer; thus the fabrication protocols have had to be re-optimised for this wavelength range. To avoid any confusion, within the paper we have added the following paragraph to

the discussion section: *“The fabrication protocol of this paper is optimised for devices targeted at an operating centre wavelength of 1550nm, however devices have also been prepared for the MidIR (2.7-3.5µm) regime using fabrication protocols based on the ones presented here.”*

As to the reviewers second point, we understand his concern but to date have not experienced any issues with our laser sources due to environmental conditions. Each of the sources used within the protocols of this paper, are commercial systems and while it is true that the tunable laser experiences some fluctuations immediately after start-up, it is sufficient to let it stabilise as described in the unit's specifications manual. Note that for the case of measurement of the group index of waveguides, we employ a broadband Amplified Spontaneous Emission light source, and thus the recorded wavelength is determined by the Optical Spectrum Analyser instead.